HHS Public Access

Author manuscript

Environ Int. Author manuscript; available in PMC 2024 September 05.

Published in final edited form as:

Environ Int. 2024 March ; 185: 108494. doi:10.1016/j.envint.2024.108494.

Long noncoding RNA ABHD11-AS1 interacts with SART3 and regulates CD44 RNA alternative splicing to promote lung carcinogenesis

Po-Shun Wang[a,b,1], **Zulong Liu**[a,b,1], **Osama Sweef**[b], **Jie Xie**[c], **Jing Chen**[d], **Haining Zhu**[d], **Patti C. Zeidler-Erdely**[e], **Chengfeng Yang**[a,b,f], **Zhishan Wang**[a,b,f,*]

[a]Stony Brook Cancer Center, Stony Brook University, Stony Brook, NY, USA

[b]Division of Cancer Biology, Department of Medicine, MetroHealth Medical Center, Case Western Reserve University School of Medicine, Cleveland, OH, USA

[c]Department of Toxicology and Cancer Biology, University of Kentucky School of Medicine, Lexington, KY, USA

[d]Department of Biochemistry and Molecular Biology, University of Kentucky School of Medicine, Lexington, KY, USA

[e]Health Effects Laboratory Division, National Institute for Occupational Safety and Health, Morgantown, WV, USA

[f]Department of Pathology, Renaissance School of Medicine, Stony Brook University, Stony Brook, NY, USA

Abstract

[*]Corresponding author at: Stony Brook Cancer Center, Department of Pathology, Stony Brook University, Stony Brook, NY, USA. zhishan.wang@stonybrook.edu (Z. Wang).

[1]These authors contribute equally to this work.

Declaration of competing interest

The authors declare that they have no known competing financial interests or personal relationships that could have appeared to influence the work reported in this paper.

Disclaimer

The findings and conclusions in this report are those of the author(s) and do not necessarily represent the official position of the National Institute for Occupational Safety and Health, Centers for Disease Control and Prevention.

Availability of data and materials

The data that support the findings of this study are available in the supplementary material of this article.

CRediT authorship contribution statement

Po-Shun Wang: Writing – review & editing, Writing – original draft, Validation, Methodology, Investigation, Formal analysis, Data curation. **Zulong Liu:** Writing – review & editing, Writing – original draft, Validation, Methodology, Investigation, Formal analysis, Data curation. **Osama Sweef:** Writing – original draft, Methodology, Investigation, Formal analysis, Data curation. **Jie Xie:** Methodology, Investigation, Data curation. **Jing Chen:** Methodology, Investigation, Data curation. **Haining Zhu:** Writing – review & editing, Writing – original draft, Methodology, Investigation, Data curation. **Patti C. Zeidler-Erdely:** Writing – review & editing, Resources, Methodology. **Chengfeng Yang:** Writing – review & editing, Writing – original draft, Supervision, Project administration, Funding acquisition. **Zhishan Wang:** Writing – review & editing, Writing – original draft, Supervision, Methodology, Investigation, Data curation, Conceptualization.

Appendix A. Supplementary data

Supplementary data to this article can be found online at https://doi.org/10.1016/j.envint.2024.108494.

Hexavalent chromium [Cr(VI)] is a common environmental pollutant and chronic exposure to Cr(VI) causes lung cancer in humans, however, the mechanism of Cr(VI) carcinogenesis has not been well understood. Lung cancer is the leading cause of cancer-related death, although the mechanisms of how lung cancer develops and progresses have been poorly understood. While long non-coding RNAs (lncRNAs) are found abnormally expressed in cancer, how dysregulated lncRNAs contribute to carcinogenesis remains largely unknown. The goal of this study is to investigate the mechanism of Cr(VI)-induced lung carcinogenesis focusing on the role of the lncRNA ABHD11 antisense RNA 1 (tail to tail) (ABHD11-AS1). It was found that the lncRNA ABHD11-AS1 expression levels are up-regulated in chronic Cr(VI) exposure-transformed human bronchial epithelial cells, chronically Cr (VI)-exposed mouse lung tissues, and human lung cancer cells as well. Bioinformatics analysis revealed that ABHD11-AS1 levels are up-regulated in lung adenocarcinomas (LUADs) tissues and associated with worse overall survival of LUAD patients but not in lung squamous cell carcinomas. It was further determined that up-regulation of ABHD11-AS1 expression plays an important role in chronic Cr(VI) exposure-induced cell malignant transformation and tumorigenesis, and the stemness of human lung cancer cells. Mechanistically, it was found that ABHD11-AS1 directly binds SART3 (spliceosome associated factor 3, U4/U6 recycling protein). The interaction of ABHD11-AS1 with SART3 promotes USP15 (ubiquitin specific peptidase 15) nuclear localization. Nuclear localized USP15 interacts with pre-mRNA processing factor 19 (PRPF19) to increase CD44 RNA alternative splicing activating β-catenin and enhancing cancer stemness. Together, these findings indicate that lncRNA ABHD11-AS1 interacts with SART3 and regulates CD44 RNA alternative splicing to promote cell malignant transformation and lung carcinogenesis.

Keywords

Hexavalent chromium; long non-coding RNA; ABHD11-AS1; SART3; USP15; CD44

1. Introduction

Toxic metals are common environmental pollutants and important etiological factors for cancer and other diseases (Yang & Wang, 2022; Zhu & Costa. 2020; Wang & Yang, 2019). Exposure to toxic metals represents a significant environmental health issue, adversely affecting human health. Hexavalent chromium [Cr(VI)] is a naturally occurring metallic element on the earth and a large amount of Cr(VI) has been released into the environment due to natural processes and human activities. As a result, Cr(VI) is a common environmental and occupational pollutant and is being listed among the “Top 20 Hazardous Substances” by the United States Agency for Toxic Substances and Disease Registry (ATSDR, 2022). Cr(VI) occupational exposure occurs at various Cr(VI) manufacturing industries. General population exposure to Cr(VI) could happen via consuming Cr(VI)-polluted water, cigarette smoking, or living close to hazardous waste facilities containing high levels of Cr (VI). Based on the convincing evidence obtained from laboratory animal studies and human epidemiology studies showing that chronic exposure to Cr(VI) causes lung cancer in experimental animals and humans, the International Agency for Research on Cancer (IARC) classified Cr(VI) as a Group I carcinogen (IARC, 1990). However, the molecular mechanism of Cr(VI) carcinogenesis has not been well understood (Wang

& Yang, 2023; Kouokam et al., 2022; Chen et al., 2019; Yatera et al., 2018). While previous studies investigated the genotoxic, epigenetic and epitranscriptomic mechanism of Cr(VI) carcinogenesis, the role of long noncoding RNA (lncRNA) dysregulation in Cr(VI) carcinogenesis remains largely unknown.

LncRNAs are a class of RNA transcripts that are longer than 200 nucleotides in length and usually do not have significant protein-coding capacities (Mattick et al., 2023; Nojima and Proudfoot, 2022; Herman et al., 2022; Wang et al., 2021). With the completion of human ENCODE projects and the advancement of next generation sequencing technologies, a large number of lncRNAs have been identified (Frankish et al., 2021). Studies showed that lncRNAs may play important roles in various physiological processes and pathogenesis based on the findings that many lncRNAs are differentially expressed at different developmental and disease stages and in different tissues (Delás and Hannon, 2017; Dey et al., 2014). For example, differential expressions of lncRNAs were found during cancer metastasis and therapies, implying that lncRNAs could play important roles in cancer progression and therapeutic responses (Adnane et al., 2022; Khawar et al., 2022; Liu et al., 2021). However, the underlying mechanisms of only a limited number of lncRNAs have now been characterized; the mechanisms of how the vast majority of dysregulated lncRNAs may contribute to cancer development and progression remain largely unknown.

ABHD11 antisense RNA 1 (tail to tail) (ABHD11-AS1, also known as LINC00035, WBSCR26, NCRNA00035) is one of up-regulated lncRNAs in several types of cancer (Golla et al., 2022). ABHD11-AS1 is localized in both cytosol and nucleus (Xue et al., 2021; Wen et al., 2019). As lncRNAs usually exhibit tissue-specific expression patterns, the up-regulation of ABHD11-AS1 levels in several types of cancer suggests that ABHD11-AS1 may have important and broad oncogenic functions. Indeed, recent studies showed that higher expression levels of ABHD11-AS1 are involved in cancer cell proliferation, migration and invasion as summarized in a recent review (Golla et al., 2022). While these recent findings suggest that ABHD11-AS1 may have oncogenic functions, the underlying mechanism has been poorly understood.

Lung cancer is the leading cause of cancer-related death, however, the mechanism of how lung cancer develops and progresses has not been well understood. Metal carcinogens are known important etiological factors for lung cancer although the mechanism of metal carcinogen exposure-caused lung cancer is unclear (Yang & Wang, 2022; Zhu & Costa. 2020; Wang & Yang, 2019). A recent study reported that ABHD11-AS1 levels are significantly increased in a small number (n = 40) of non-small cell lung cancer (NSCLC) tissues and higher ABHD11-AS1 levels are associated with a worse overall survival of lung cancer patients (Xue et al., 2021), suggesting that ABHD11-AS1 may play an important role in lung cancer. Nonetheless, the expression levels of ABHD11-AS1 and its role in metal carcinogen-induced lung carcinogenesis, different stages of lung carcinogenesis and different subtypes of lung cancers have not been studied. The aim of this study is to investigate the mechanism of Cr(VI) carcinogenesis focusing on the biological role of ABHD11-AS1 in lung carcinogenesis. By using bioinformatical, chemical, genetic, cellular and molecular approaches, we found that ABHD11-AS1 is up-regulated in Cr(VI)-transformed cells and Cr(VI)-exposed mouse lung tissues, human lung adenocarcinomas

(LUADs), but not in human lung squamous cell carcinomas (LUSCs). We further determined that ABHD11-AS1 directly binds to RNA-binding protein SART3 (Spliceosome Associated Factor 3, U4/U6 Recycling Protein) and demonstrated that ABHD11-AS1 interacts with SART3 and regulates CD44 RNA alternative splicing to promote cell malignant transformation, cancer stem cell-like property and lung carcinogenesis.

2. Materials and methods

2.1. Cell lines and cell culture

Immortalized human bronchial epithelial BEAS-2B cell line and human non-small lung cancer cell lines were purchased from America Type Culture Collection (ATCC, Manassas, VA). The primary normal human bronchial epithelial cells (NHBE) were obtained from Lonza (Walkersville, MD) and cultured in bronchial epithelial growth medium (Lonza). BEAS-2B and lung adenocarcinoma A549, H1975, H2009, H2030 and PC9/GR4 cells were cultured in Dulbecco's Modified Eagle Medium (DMEM) (Thermo Fisher, Waltham, MA) supplemented with 5 % fetal bovine serum (FBS) (Sigma-Aldrich, St. Louis, MO) and 1 % Penicillin-Streptomycin (P/S) (10,000U/mL) (Thermo Fisher). Lung adenocarcinoma H460 and H1299 cells, lung squamous cell carcinoma H157, H520, H2450 and HCC15 cells were cultured in Rosewell Park Memorial Institute (RPMI)-1640 Medium (Thermo Fisher) supplemented with 5 or 10 % FBS and 1 % P/S. All cells were maintained at 37 °C in a humidified atmosphere of 5 % CO_2 and sub-cultured every 2 ~ 3 days by adding 0.25 % Trypsin-EDTA (Thermo Fisher).

2.2. Cell transformation by chronic Cr(VI) ($K_2Cr_2O_7$) exposure

BEAS-2B parental cells were initially treated with $K_2Cr_2O_7$ in a dose-dependent manner (0.125, 0.25, 0.5 and 1 μM) for 72 h to determine the cytotoxic effect of Cr(VI). It was found that the highest dose of exposure to $K_2Cr_2O_7$ for 72 h that had no significant effect on either cell viability or proliferation was 0.25 μM of $K_2Cr_2O_7$. Hence, cells were exposed to this Cr(VI) dose for 20 weeks to induce cell transformation followed by determining the phenotypes with soft agar colony-forming assay, sphere-forming assay and mouse xenograft tumorigenesis model (Wang et al., 2022; Clementino et al., 2020; Wang et al., 2019b; Wang et al., 2018a). The passage-matched control and chronic Cr(VI) exposure-transformed BEAS-2B cells were designated as BEAS-2B-Control and BEAS-2B-Cr(VI), respectively.

2.3. Chronic Cr(VI) exposure in mice

Mouse chronic Cr(VI) exposure through oropharyngeal aspiration was performed in Dr. Patti C Zeidler-Erdely's Laboratory at the National Institute for Occupational Safety and Health (Morgantown, WV). The detailed Cr(VI) ($CaCrO_4$) exposure protocol, justification for the dose of calcium chromate exposure, and Cr(VI)-induced lung tumorigenesis in mice were reported in our previous publication (Zeidler-Erdely et al., 2020). Animals were euthanized at the end of the experiment, vehicle control-and chromate-exposed mouse lungs were immediately frozen at −80 °C for further RNA and protein assays or immersed in 10 % neutral-buffered formalin (NBF), followed by paraffin-embedding and tissue-sectioning for immunofluorescence (IF) and immunohistochemistry (IHC) staining.

2.4. Generation of gene stable overexpression and knockdown cells

The lentiviral particles purchased from Transomic Technologies (Huntsville, AL) for the vector control and ABHD11-AS1 knockdown were used to generate vector control and ABHD11-AS1 stable knockdown cells, following the procedures described in our previous publications (Wang et al., 2019b, 2022). The sequences of ABHD11-AS1 wildtype full length, ABHD11-AS1 antisense RNA strand and ABHD11-AS1 mutant (with SART3 binding site mutated) were synthesized by GenScript (Piscataway, NJ) and subcloned into pLenti6.3 lentiviral vector (named as pLenti6.3-ABHD11-AS1, pLenti6.3-ABHD11-AS1-as and pLenti6.3-ABHD11-AS1-Mut, respectively). The mutated region including a highly conserved ACAGAG *hexa*-nucleotide was thought to be SART3 binding site (Bell et al., 2002). The pLenti6.3 vector control, pLenti6.3-ABHD11-AS1, pLenti6.3-ABHD11-AS1-as and pLenti6.3-ABHD11-AS1-Mut lentiviral particles were used to generate the vector control, ABHD11-AS1, ABHD11-AS1-as, and ABHD11-AS1-Mut stable overexpression cells. The USP15 and CD44 isoform 1 (including all variant exons; CD44v) cDNAs were purchased from Addgene (Watertown, MA). To overexpress USP15 or CD44v in ABHD11-AS1-as overexpressing cells, the cDNA sequences of USP15 or CD44v were subcloned into pLenti7.3 lentiviral vector, and the corresponding overexpressing cells were further sorted out by fluorescence-activated cell sorting (FACS) using GFP as the selection marker. The overexpression or knockdown of ABHD11-AS1 levels were evaluated by qPCR assay. The USP15 or CD44v over-expressions were determined by Western blot analysis.

2.5. Soft agar colony formation assay, serum-free suspension culture sphere formation assay and ALDEFLUOR assay

The soft agar colony formation assay and serum-free suspension culture sphere formation assay were performed according to the procedures described in our previous articles (Wang et al., 2020; Wang et al., 2019a; Xiao et al., 2018; Yang et al., 2005). The ALDEFLUOR assay was performed by using the ALDEFLUOR Kit (Stem Cell Technologies, Vancouver, BC) following the manufacturer's protocol.

2.6. RNA isolation, qPCR and Western blot analysis

Total RNA was extracted by TRIzol reagent (Thermo Fisher, MA) according to the manufacturer's instructions and RNA concentrations were measured by NanoDrop spectrophotometer (Thermo Fisher). TaqMan Gene Expression Assays were performed on the QuantStudio 3 Real-Time PCR Platform (Applied Biosystems). The $2^{-\Delta\Delta ct}$ method was utilized to determine the relative RNA expression levels of target genes, with human gene *RN18S1* as the endogenous control. Additionally, Western blot was performed following our published protocols (Wang et al., 2012, 2013, 2014) and raw data images were captured by Azure 600 Imaging System (Azure Biosystems, Dublin, CA). All primary antibodies used in Western Blot are listed in Supplementary Table 1. Protein band intensities were further quantitated by AzureSpot Pro (Azure Biosystems) and ImageJ software.

2.7. Immunohistochemistry (IHC) and immunofluorescence (IF) staining

The IHC staining was performed by using the VECTASTAIN Elite ABC Universal Kit (Vector Laboratories, Newark, CA) according to the manufacturer's instructions. Briefly,

tissue slides were deparaffinized and hydrated through xylene and graded alcohol series. Antigen retrieval was then performed by autoclave heating for 15 min in citrate-based retrieval solution. The enzymatic activity of endogenous peroxidase was further quenched by incubation in BLOXALL™ Blocking Solution at room temperature (RT) for 10 min. Tissue sections were incubated overnight at 4 °C with primary antibodies and counter stained with hematoxylin solution. For IF staining, cells were seeded on cover glasses in 6-well plates and incubated at 37 °C for 24 h. Briefly, cells were firstly washed with 1X PBS, fixed with 4 % paraformaldehyde for 15 min and permeabilized with 1 % Triton X-100 for 15 min. Next, cells were blocked with 3 % bovine serum albumin (BSA) for 30 min. The primary antibodies were diluted with 1 % BSA and incubated at 4 °C overnight, followed by intubating with Alexa-Fluor® fluorescent secondary antibodies at RT for 1 h. At the end of incubation, cells were washed with 1X PBS and stained with 4,6-diamidino-2-phenylindole (DAPI) for 10 min to visualize the nuclei. The IF staining images were captured by a Nikon fluorescent microscope (ECLIPSE T*i*2) or a Leica THUNDER Imaging System. All primary antibodies used in IHC and IF are shown in Supplementary Table 1.

2.8. Nude mouse xenograft tumorigenesis study

Cr(VI)-transformed cells (1.5×10^6) or human lung cancer cells (A549: 1.0×10^6; H460-shControl and H460-shABHD11-AS1 cells: 5.0×10^5; H460-Control and H460-ABHD11-AS1-as cells: (5.0×10^5, 5.0×10^4, 5.0×10^3); H460-ABHD11-AS1-as-vector control and H460-ABHD11-AS1-as-CD44v cells (5.0×10^4) suspended in 0.1 mL of 1:1 growth factor-reduced Matrigel and serum-free DMEM were subcutaneously injected into the flanks of 6-week-old female nude mice (Charles River Laboratories, Wilmington, MA). Mice injected with Cr(VI)-transformed cells, A549 cells or H460 cells were euthanized at 12, 5 and 3 weeks post-inoculation, respectively. The xenograft tumors from each mouse were harvested, weighed and photographed. Animals were maintained under specific pathogen-free conditions, and animal protocols were reviewed and approved by the University of Kentucky and Case Western Reserve University Institutional Animal Care and Use Committee (IACUC).

2.9. Cell fractionation assay

Subcellular protein fractionation assay was performed by using NE-PER Nuclear and Cytoplasmic Extraction Reagents (Thermo Fisher) following the manufacturer's instructions. Briefly, cell pellets were resuspended with ice-cold cytoplasmic extraction reagent I (CER I) and incubated on ice for 10 min after vigorous vortex. The mixture was then added with CER II, spun down at 12,000 rpm at 4 °C for 5 min and the cytoplasmic extract was transferred to a fresh tube. The nuclear pellets were further incubated with nuclear extraction reagent (NER) containing protease inhibitor followed by sonication. The cytoplasmic and nuclear proteins were applied to Bio-Rad DC™ Protein Assay (Bio-Rad, Hercules, CA) to determine protein concentrations before standard Western blot analysis.

2.10. Immunoprecipitation (IP) and co-immunoprecipitation (co-IP) analysis

Cell pellets were initially lysed by using Lysis Buffer I (20 mM Tris HCl, 100 mM NaCl, 0.5 % NP-40 and 0.5 mM EDTA (pH 7.4), adding 1 mM PMSF and the protease inhibitor cocktail before use). After incubating on ice for 10 min, cell lysates were centrifuged at

13,000 rpm at 4°C for 10 min. The supernatants were collected, pre-cleared and incubated with primary antibodies at 4°C overnight with gentle rotation. Protein A/G PLUS-Agarose (Santa Cruz Biotechnology, Dallas, TX) were washed with Lysis Buffer I three times and added into protein tubes rotating at 4 °C for 2 h. Subsequently, beads were spun down and washed stringently with Lysis Buffer II (20 mM Tris HCl, 100 mM NaCl, 1 % NP-40 and 0.5 mM EDTA (pH 7.4). The precipitated protein complexes were analyzed by standard Western blot.

2.11. In vitro transcription and RNA pulldown assay

The expression plasmids of pBluescript II-SK-ABHD11-AS1 and its antisense pBluescript II-SK-ABHD11-AS1-as were purchased from GenScript (Piscataway, NJ) and linearized by EcoRI-HF (New England BioLabs, Ipswich, MA), followed by *in vitro* transcription for RNA synthesis of biotinylated ABHD11-AS1 or ABHD11-AS1-as. The lncRNA pulldown assay was then conducted to determine putative binding partners of ABHD11-AS1. Briefly, 4 μg of linearized plasmids were added into mixture (Biotin RNA Labeling Mix (Roche, Basel, Switzerland), T7 RNA polymerase (Promega, Madison, WI) and 5X Transcription Buffer), incubated at 37 °C for 3 h and proceeded to RNase-free DNase I (Roche) digestion at 37 °C for 15 min. Biotinylated RNAs were further purified by G-50 Sephadex Columns (Roche). Subsequently, RNA pulldown was carried out by incubating 20 μg of biotinylated RNAs with BEAS-2B-Cr (VI) protein lysate at 4 °C for 1 h, and protein-bead complexes were resuspended with sample buffer and boiled for 10 min. Protein supernatant was applied to Western blot analysis after centrifugation.

2.12. Liquid chromatography-electrospray ionization-tandem mass spectrometry (LC-ESI-MS/MS) analysis and MS/MS protein identification

All mass spectra reported in this study were acquired by University of Kentucky Proteomics Core Facility. The protein gel bands were initially excised and subjected to dithiothreitol reduction, iodoacetamide alkylation, and in-gel trypsin digestion by a standard protocol. The resulting tryptic peptides were extracted, concentrated and subjected to shot-gun proteomics analysis as previously described (Kamelgarn et al., 2018). LC-MS/MS analysis was performed using an LTQ-Orbitrap Mass Spectrometer (Thermo Fisher) coupled with an Eksigent Nanoflex cHiPLC™ System (Eksigent, Dublin, CA) through a nano-electrospray ionization source. The peptide samples were separated with a reversed phase cHiPLC column (75 μm × 150 mm) at a flow rate of 300 nL/min. Mobile phase A was water with 0.1 % (v/v) formic acid while B was acetonitrile with 0.1 % (v/v) formic acid. A 50 min gradient condition was applied: initial 3 % mobile phase B was increased linearly to 40 % in 24 min and further to 85 % and 95 % for 5 min each before it was decreased to 3 % and re-equilibrated. The mass analysis method consisted of one segment with eleven scan events. The first scan event was an Orbitrap MS scan (300–1800 m/z) with 60,000 resolutions for parent ions followed by data-dependent MS/MS for fragmentation of the 10 most intense multiple charged ions with collision-induced dissociation (CID) method.

The LC-MS/MS data were submitted to a local mascot server for MS/MS protein identification via Proteome Discoverer (PD) platform (Thermo Fisher) against a custom database containing reviewed Homo sapiens from UniPort (downloaded 01/04/2020,

with a total of 20,367 proteins). Typical parameters used in the MASCOT MS/MS ion search included: trypsin digestion with a maximum of two miscleavages, cysteine carbamidomethylation and methionine oxidation, 10 ppm precursor ion and 0.8 Da fragment ion mass tolerances. A decoy database was built and searched. Filter settings that determine false discovery rate (FDR) are used to distribute the confidence indicators for the peptide matches. Ultimately, peptide matches that pass the filter associated with the FDR rate of 1 % and 5 % are assigned as high and medium confident peptides, respectively.

2.13. RNA-seq analysis

Total RNAs from H460 cells transfected with control siRNA, PRPF19- or USP15-targeting siRNAs (100 nM, 48 h), from chronic Cr(VI) exposure-transformed BEAS-2B cells [BEAS-2B-Cr(VI)] and the passage-matched control BEAS-2B cells (BEAS-2B-Control), were submitted to BGI Genomics (Cambridge, MA) for RNA-seq analysis. RNA-seq raw data were further analyzed by BGI bioinformatics services. Differentially-expressed genes (DEGs) between H460-siControl and H460-siPRPF19, H460-siControl and H460-siUSP15, BEAS-2B-Control and BEAS-2B-Cr (VI), were further used for gene ontology (GO) and gene set enrichment analyses (GSEA). RNA alternative splicing profiles from H460-siControl, H460-siPRPF19 and H460-siUSP15 cells were used for mRNA alternative spicing analyses.

2.14. Bioinformatics analysis

ABHD11-AS1 expression levels in various types of cancer and their corresponding normal tissues were analyzed using Gene Expression Profiling Interactive Analysis (GEPIA) platform (http://gepia.cancer-pku.cn/) (Tang et al., 2017; Li et al., 2021).

For prognostic and diagnostic analysis, the expression profile of ABHD11-AS1 in patients with lung adenocarcinoma (LUAD) and lung squamous cell carcinoma (LUSC) were obtained from TCGA_LUAD and TCGA-LUSC project datasets (https://portal.gdc.cancer.gov/projects/TCGA-LUAD and https://portal.gdc.cancer.gov/projects/TCGA-LUSC), respectively. The prognostic and diagnostic value of ABHD11-AS1 were explored through overall survival analysis and receiver operating characteristic (ROC) curve analysis, respectively. MedCalc statistical platform (https://www.mdcalc.com/ accessed on 11/03/2022) was used to explore the prognostic performance via overall-survival analysis of lung cancer patients. ROC curves were conducted using the pROC package in the R programming language, version 4.2.1, on a Windows 10 operating system (https://www.rstudio.com/ (accessed on 25 October 2022). The computation aimed to determine the Area Under the Curve (AUC), a widely employed metric for assessing the discriminative ability of diagnostic tests and predictive models.

The gene ontology analyses of DEGs between H460-siControl and H460-siUSP15; H460-siControl and H460-siPRPF19 cells retrieved from our RNA-seq data were performed to explore biological processes (BP) potentially changed after silencing either USP15 or siPRPF19. BPs were implemented with ToppGene (https://toppgene.cchmc.org/ (accessed on 11/10/2022). RNA alternative splicing profiles were obtained from our RNAseq data of H460-siCtrl, H460-siUSP15 and H460-siPRPF19 cells. Prism 8 statistical software

(GraphPad Software, Boston, MA) was used to calculate the splicing event numbers, including alternative 5′ splicing site (A5SS), alternative 3′ splicing site (A3SS), mutually exclusive exons (MXE), retained intron (RI) and skipped exon (SE).

In addition, DEGs between BEAS-2B-Control and BEAS-2B-Cr(VI); H460-siControl and H460-siUSP15; H460-siControl and H460-siPRPF19 cells obtained from our RNA-seq data were used for gene set enrichment analysis (GSEA) in oncogenic and stemness gene sets from C2 and C5 collections from the Molecular Signatures Database (MSigDB) (https://www.gsea-msigdb.org/gsea/msigdb/index.jsp (accessed on 10/20/2022). Python Programming Language (https://www.python.org/ (accessed on 10/26/2022) was used for GSEA via the GSEA package. Furthermore, whole-exon expression profiles of LUAD and LUSC were obtained from TCGA_LUAD and TCGA-LUSC project datasets, respectively. MedCalc statistical platform (https://www.mdcalc.com/ (accessed on 11/03/2022) was used to analyze the correlation between the ratio of CD44s/CD44v and individual genes.

2.15. Statistical analysis

The statistical analyses for the significance of differences in presented numerical data (mean ± SD) were carried out by Prism 8 (GraphPad Software, San Diego, CA) testing different treatment effects using two-tailed *t* tests for the comparison of two data sets. The significance of the difference in nude mouse xenograft tumor incidence rate was tested using Fisher's exact test. A p value of < 0.05 was considered statistically significant.

3. Results

3.1. ABHD11-AS1 levels are up-regulated in different stages of lung carcinogenesis playing an important role in tumorigenesis

To investigate the biological role of ABHD11-AS1 in lung cancer, we sought to determine whether ABHD11-AS1 has been involved in different stages of lung carcinogenesis. We firstly analyzed ABHD11-AS1 levels in chronic Cr(VI) exposure-transformed human bronchial epithelial cells representing the early stage of lung carcinogenesis and in well-established eleven human lung cancer cells representing the later stage of lung carcinogenesis. We used BEAS-2B cells that were malignantly transformed by chronic exposure to a low dose of Cr(VI) for 20 weeks and lungs of mice chronically-exposed to Cr(VI) for 26 weeks (1 exposure/week). Cr(VI) has been known as a well-established lung cancer etiological factor (Wang & Yang, 2023; Kouokam et al., 2022; Chen et al., 2019; Yatera et al., 2018). A detailed description for Cr(VI) exposure both *in vitro* and *in vivo*, characterization of Cr(VI) exposure-caused cell malignant transformation, and mouse lung tumorigenesis were reported in our previous articles (Wang et al., 2022; Clementino et al., 2020; Wang et al., 2019b; Wang et al., 2018a; Zeidler-Erdely et al., 2020). As shown in Fig. 1a, the expression level of ABHD11-AS1 was significantly increased in Cr(VI)-transformed human bronchial epithelial cells [BEAS-2B-Cr(VI)] and chronically Cr(VI)-exposed mouse lung tissues. Next, we analyzed ABHD11-AS1 level in a panel of human lung cancer cells and primary normal human bronchial epithelial (NHBE) cells. We found that ABHD11-AS1 levels in lung adenocarcinoma (LUAD) cells were significantly higher than NHBE cells

(Fig. 1b). However, no increases of ABHD11-AS1 level in lung squamous cell carcinoma (LUSC) cells were observed when compared to NHBE (Fig. 1b).

To determine whether ABHD11-AS1 up-regulation has an important role in lung cancer development and progression, we used a loss of function approach to determine the role of ABHD11-AS1 in Cr(VI)-induced cell malignant transformation and lung cancer cell tumorigenesis. We initially used ABHD11-AS1-targeting small interfering RNAs (siRNAs) to knock down ABHD11-AS1 level in those cells already transformed by chronic Cr(VI) exposure. It was found that ABHD11-AS1 knockdown in BEAS-2B-Cr(VI) cells significantly reduced their capability to form suspension spheres (Fig. 1c), an indication of loss of cancer stem cell (CSC)-like property (Wang et al., 2019b). We next stably knocked down ABHD11-AS1 by ABHD11-AS1-targeting short hairpin RNAs (shRNAs) (Fig. 1d). As shown in Fig. 1e, ABHD11-AS1 stable knockdown significantly reduced the capability of Cr(VI)-transformed cells to produce xenograft tumors in nude mice as all mice injected with shRNA control (shCtrl) cells produced tumors but only 1 out of 5 mice in ABHD11-AS1 knockdown (shABHD11-AS1) group had tumor (Fig. 1e). These results indicated that high ABHD11-AS1 level is involved in maintaining the malignant phenotype of Cr(VI)-transformed cells.

Meanwhile, we determined the effect of stable knockdown of ABHD11-AS1 in parental non-transformed human bronchial epithelial cells on the ability of chronic Cr(VI) exposure to induce cell malignant transformation. As shown in Fig. 1f, ABHD11-AS1 knockdown significantly reduced the capability of chronic Cr(VI) exposure to induce cell transformation as evidenced by the significantly less numbers of soft agar colonies and suspension spheres formed by Cr(VI)-exposed ABHD11-AS1 knockdown cells. These results indicated that up-regulation of ABHD11-AS1 contributes causally to chronic Cr(VI) exposure-induced malignant transformation of human bronchial epithelial cells, suggesting that ABHD11-AS1 up-regulation may play an important role in the early stage of lung carcinogenesis.

Furthermore, we determined the effects of ABHD11-AS1 knockdown on well-established human lung cancer cells' cancer stem cell (CSC)-like property and tumorigenicity. As shown in Fig. 1g and 1 h, stable knockdown of ABHD11-AS1 in human LUAD H460 cells significantly reduced their CSC-like property as determined by significant decreases of sphere number and aldehyde dehydrogenase (ALDH)-positive cell population. These results suggested that high ABHD11-AS1 levels play a crucial role in maintaining CSC-like property of human lung cancer cells. This was further supported by mouse xenograft tumorigenesis experiment showing that injection of ABHD11-AS1 knockdown H460 cells produced significantly smaller tumors in nude mice when compared to control cells (Fig. 1i). To reinforce this point, we also used human LUAD A549 cells and another approach of loss of function by stably expressing the antisense RNA of ABHD11-AS1 (ABHD11-AS1-as) in A549. It was found that injection of A549-ABHD11-AS1-as cells produced less and significantly smaller tumors in mice than the injection of control cells (Fig. 1j). Finally, we generated H460-ABHD11-AS1-as stable expression cells and performed the limited dilution tumorigenesis assay to further demonstrate the importance of ABHD11-AS1 in maintaining cancer stemness. As shown in Supplementary Fig. 1, ABHD11-AS1-as-H460 cells exhibited weaker tumorigenicity when 5×10^5 or 5×10^4 of cells were injected. Strikingly, when $5 \times$

10^3 of cells were injected, none of mice injected with H460 cells expressing ABHD11-AS1-as grew any tumors while 50 % of mice injected with control cells had tumors.

Taken together, our findings showed that high levels of ABHD11-AS1 not only contributed causally to Cr(VI)-induced cell malignant transformation, ABHD11-AS1 up-regulation also played an important role in maintaining CSC-like property and tumorigenicity both in Cr(VI)-transformed cells and human lung cancer cells. These findings suggested that ABHD11-AS1 may play an important role in lung cancer development and progression.

3.2. ABHD11-AS1 levels are up-regulated and associated with worse prognosis in lung adenocarcinomas but not in lung squamous cell carcinomas

To determine the relevance of above findings obtained from both Cr (VI) exposure-transformed cells and lung cancer cells to human lung cancer, we analyzed ABHD11-AS1 levels in 9,736 tumors and 8,587 normal tissues by GEPIA platform. As shown in Fig. 2a, ABHD11-AS1 levels were up-regulated in 21 of 33 types/subtypes of cancer analyzed. Interestingly, ABHD11-AS1 levels were drastically higher in lung adenocarcinomas (LUADs, n = 483) when compared to normal lung tissues (n = 347) (Fig. 2a). In contrast, no obvious difference of ABHD11-AS1 level was observed between lung squamous cell carcinomas (LUSCs, n = 486) and normal lung tissues (n = 338) (Fig. 2a). These bioinformatics analysis findings were consistent with our results presented in Fig. 1b, showing that ABHD11-AS1 levels were up-regulated in LUAD cells but not in LUSC cells. In addition, ABHD11-AS1 levels were also significantly higher in late-stage lung cancers than early-stage lung cancers (Supplementary Fig. 2a). Moreover, similar results were observed by analyzing additional data sets (Supplementary Fig. 2b). Meanwhile, Kaplan–Meier survival and Receiver Operating Characteristic curve (ROC) analyses were performed to determine the significance of ABHD11-AS1 abnormal expression in lung cancer. As shown in Fig. 2b, higher expressions of ABHD11-AS1 were associated with a significantly worse overall survival in LUAD patients. However, no such a correlation was found in patients with LUSC (Fig. 2c). Similarly, the ROC analyses revealed that ABHD11-AS1 levels displayed a significantly higher accuracy, sensitivity, and specificity for the diagnosis of LUAD than LUSC (Fig. 2d and 2e). Collectively, our findings from above bioinformatics analyses indicated that ABHD11-AS1 level was up-regulated in many types/subtypes of cancer. Specifically, ABHD11-AS1 expression was significantly increased in LUADs, but not in LUSCs. Moreover, high levels of ABHD11-AS1 were associated with significantly worse overall survival and represented a significant diagnostic value among LUAD patients, providing additional evidence supporting that ABHD11-AS1 may have critical functions in lung carcinogenesis.

3.3. ABHD11-AS1 directly interacts with SART3

We next sought to determine the underlying mechanism of how ABHD11-AS1 may promote lung cancer development and progression. One of the known mechanisms for lncRNA functionality is to interact with RNA-binding proteins (RBPs) (Shaath et al., 2022; Schmitt and Chang, 2016; Wang et al., 2011). Generally, specific RBPs for some annotated lncRNAs have been identified, which play key roles in mediating biological functions of lncRNAs (Shaath et al., 2022; Schmitt and Chang, 2016; Wang et al., 2011).

Therefore, we decided to identify new and functional protein-binding partners for ABHD11-AS1. After performing *in vitro* transcription and RNA pulldown assays (A representative protein gel image from an RNA pulldown assay was shown in Fig. 3a), the putative protein-binding partners for ABHD11-AS1 and ABHD11-AS1-as were identified by using mass spectrometry analysis (Supplementary Table 2). Based on the numbers of unique peptides identified from ABHD11-AS1 and ABHD11-AS1-as pulldown assays, we selected top five candidates for further verification. As shown in Fig. 3b, our candidate protein showing the largest difference bound between ABHD11-AS1 and ABHD11-AS1-as (as negative control) was SART3 (Spliceosome Associated Factor 3, U4/U6 Recycling Protein). SART3 peptide fingerprint from the mass spectrometry analysis was shown in Supplementary Fig. 3. While SART3 protein levels were increased in Cr (VI)-transformed cells, stably overexpressing ABHD11-AS1 or ABHD11-AS1-as did not significantly affect SART3 protein among human bronchial epithelial cells, Cr(VI)-transformed cells or human lung cancer cells (Fig. 3c and 3d).

We next stably knocked down SART3 expression in Cr(VI)-transformed cells and human lung cancer cells followed by evaluating the effects of SART3 down-regulation on their malignant phenotypes. It was found that SART3 knockdown in Cr(VI)-transformed cells had no effect on ABHD11-AS1 level but significantly reduced cell abilities to grow soft agar colonies and suspension spheres (Fig. 3e to 3 h). Similarly, ABHD11-AS1 level was unaffected after SART3 knockdown in human lung cancer A549 cells but significantly reduced its capability of growing xenograft tumors in nude mice (Fig. 3i to 3 k). In conclusion, these findings suggested that the interaction of ABHD11-AS1 with SART3 might play an important role in lung carcinogenesis.

3.4. ABHD11-AS1 and SART3 interaction promotes USP15 nuclear localization

Previous reports have revealed that SART3 interacts with deubiquinase USP15 (Ubiquitin-Specific Peptidase 15) and promotes its nuclear localization to regulate RNA alternative splicing (Zhang et al., 2016; Das et al., 2019). However, it remains unknown whether the interaction between ABHD11-AS1 and SART3 plays an important role in the promotive effect of SART3 on USP15 nuclear localization. More importantly, dysregulation of protein subcellar localizations may affect various signaling pathways involved in cancers. We thus investigated the ABHD11-AS1-SART3 effect on USP15 nuclear localization. Our data showed that USP15 nuclear localization was increased in Cr(VI)-transformed cells as determined by cell fractionation assay and USP15 immunofluorescent staining (Fig. 4a and 4b). SART3 knockdown did not affect total level of USP15 but significantly reduced its nuclear localization in Cr(VI)-transformed cells (Fig. 4c). Similarly, knockdown of SART3 also significantly decreased nuclear level of USP15 in A549 cells (Fig. 4d). We further manipulated ABHD11-AS1 level and determined its effect on USP15 nuclear localization. Our results showed that ABHD11-AS1 over-expression in non-transformed human bronchial epithelial cells increased USP15 nuclear level (Fig. 4e to 4f). In contrast, stably expressing the antisense RNA of ABHD11-AS1reduced USP15 nuclear level significantly in both Cr(VI)-transformed cells and human lung cancer cells (Fig. 4g to 4j). Together, these findings along with the results presented in Fig. 3a–3b showing that the antisense RNA of ABHD11-AS1 (ABHD11-AS1-as) did not interact with SART3, and the results presented

in Fig. 3c to 3f showing no effect of SART3 knockdown on ABHD11-AS1 levels and no effect of manipulating ABHD11-AS1 on SART3 levels suggested, on one hand, that the interaction between ABHD11-AS1 and SART3 could play an important role in USP15 nuclear recruitment. These findings, On the other hand, could not rule out the possibility that ABHD11-AS1 may promote USP15 nuclear localization by modifying either SART3 or USP15 to increase SART3-USP15 interaction through undefined mechanisms.

3.5. ABHD11-AS1 and SART3 increase the interaction of USP15 with RNA splicing factor PRPF19

Previous study reported that nuclear-localized USP15 regulates the process of RNA alternative splicing through interacting with and deubiquitylating splicing factors (Das et al., 2017). We next determined the effect of manipulating either ABHD11-AS1 or SART3 on the interaction between USP15 and several RNA splicing factors. Our co-IP data showed that stably overexpressing ABHD11-AS1 in non-transformed human bronchial epithelial cells drastically increased the interaction of USP15 with splicing factor PRPF19 (Pre-mRNA Processing Factor 19) (Fig. 5a). PRPF19 regulates splicing event through interacting with CDC5L (Cell Division Cycle 5-Like) to form a multi-component complex known as PRPF19/CDC5L complex (Grote et al., 2010). ABHD11-AS1 over-expression in non-transformed human bronchial epithelial cells also greatly increased the interaction of USP15 with CDC5L (Fig. 5a). In contrast, stably expressing the antisense RNA of ABHD11-AS1 (ABHD11-AS1-as) or stably knocking down SART3 in Cr(VI)-transformed human bronchial epithelial cells significantly reduced the interaction of USP15 with PRPF19 and CDC5L (Fig. 5b to 5c). Furthermore, the interactions of USP15 with PRPF19, Cdc5L and other splicing factors were drastically reduced in BEAS-2B cells stably overexpressing an ABHD11-AS1 mutant with SART3 interacting site mutated, comparing to BEAS-2B cells stably overexpressing wildtype ABHD11-AS1 (Fig. 5d). Similarly, overexpression of the mutant ABHD11-AS1 in LUAD A549 cells also significantly reduced the interactions of USP15 with PRPF19 and CDC5L (Fig. 5e). These results suggested an important role of ABHD11-AS1 and SART3 interaction in regulating USP15′s interactions with PRPF19 and other splicing factors.

Since manipulating ABHD11-AS1 or SART3 displayed dramatic and consistent effects on the interaction between USP15 and PRPF19 (Fig. 5a to 5e), we further determined nuclear level of PRPF19 and the effects of manipulating ABHD11-AS1, SART3 or USP15 expression on nuclear PRPF19 levels. It was found that overexpressing ABHD11-AS1 increased nuclear PRPF19 protein levels (the input PRPF19 level) (Fig. 6a). In contrast, SART3 or USP15 knockdown (Fig. 6 b and 6d) or overexpressing an ABHD11-AS1 antisense (Fig. 6e) or mutant with SART3 binding site mutated (Fig. 6c) reduced nuclear PRPF19 protein levels (the input PRPF19 level). Moreover, the effect of overexpressing ABHD11-AS1 antisense RNA on nuclear PRPF19 level was reversed by overexpressing USP15 (Fig. 6e). These results along with that shown in Fig. 4a–4 g revealed a nice positive correlation between nuclear USP15 and PRPF19 protein levels, supporting a role of nuclear USP15 stabilizing PRPF19 protein. In addition, the IP experiments showed that overexpressing ABHD11-AS1 increased the precipitated nuclear PRPF19 level (Fig. 6a), while SART3 or USP15 knockdown (Fig. 6 b and 6d) or overexpressing an ABHD11-

AS1 antisense (Fig. 6e) or mutant with SART3 binding site mutated (Fig. 6c) reduced the precipitated nuclear PRPF19 protein levels. These results suggested that manipulating ABHD11-AS1, SART3 or USP15 may change nuclear PRPF19 conformation and activation status. Furthermore, it was found that nuclear PRPF19 and USP15 levels in chronic Cr(VI) exposure-induced mouse lung tumor tissues were significantly higher than PBS-exposed mouse lung tissues (Fig. 6f–6 g). Collectively, our results suggested that increased nuclear level of USP15 could have a pivotal role in stabilizing splicing factor PRPF19 and activating the PRPF19 complex to regulate RNA splicing.

3.6. USP15 and PRPF19 mediate the effect of ABHD11-AS1 on CD44 alternative splicing to increase the expression of CD44v6

Next, we used siRNAs specifically targeting either PRPF19 or USP15 in H460 cells followed by RNA-seq analysis to investigate the potential changes in RNA splicing. Our GO analyses showed that RNA alternative splicing and processing were among top biological processes changed by knocking down PRPF19 or USP15 (Supplementary Fig. 4). Indeed, our bioinformatics analyses also revealed that PRPF19 or USP15 knockdown significantly changed the number of RNA alternative splicing events (Supplementary Fig. 5). Intriguingly, one of the most dramatic changes was the drastically increase of skip of exons (SE), resulting from silence of PRPF19 or USP15 (Supplementary Fig. 5).

The increase of SE event could reduce the expression of gene variants. One of genes that have multiple exons and expressions of its variants involved in cancer is *CD44*, a well-known CSC marker and driver (Hassn Mesrati et al., 2021; Chen et al., 2018; Yan et al., 2015). Human CD44 pre-mRNA has 10 standard exons and 9 variant exons. Previous studies showed that expression of CD44 variant 6 (CD44v6) plays an important role in producing and maintaining cancer stemness, thereby promoting cancer development and progression (Ma et al., 2019; Wang et al., 2018b). We further examined whether chronic Cr(VI) exposure or manipulating the levels of ABHD11-AS1, USP15 or PRPF19 influences CD44v6 expression. It was found that CD44v6 protein level was increased in chronic Cr(VI) exposure-transformed cells (Fig. 7a). Similarly, CD44v6 RNA level in Cr(VI)-exposed mouse lung tissues was significantly increased when compared to corresponding control group (Fig. 7b). In addition, IF staining of CD44v6 showed a high level of CD44v6 in Cr(VI) exposure-induced mouse lung tumors (Supplementary Fig. 6). Moreover, stably overexpressing ABHD11-AS1 in non-transformed human bronchial epithelial cells or in human LUSC HCC15 cells increased CD44v6 protein levels (Fig. 7c). In contrast, stably expressing the antisense RNA of ABHD11-AS1 in Cr(VI)-transformed cells or human LUAD A549 and H460 cells greatly reduced their CD44 and CD44v6 protein levels (Fig. 7d). Our findings were also supported by additional bioinformatics analysis showing that ABHD11-AS1 levels were negatively correlated with the ratio of level of CD44 standard form to CD44 variant forms (CD44s/CD44v) in LUADs, but not in LUSCs (Supplementary Fig. 7a).

Consistent with our findings of bioinformatics analysis showing that knockdown of either USP15 or PRPF19 significantly increased SE event, our qPCR and Western blot analyses also revealed that USP15 or PRPF19 knockdown in A549 and H460 cells significantly

decreased their CD44v6 mRNA and protein levels (Fig. 7e to g). Furthermore, silence of USP15 or PRPF19 in ABHD11-AS1 overexpressing cells also reversed the effect of ABHD11-AS1 overexpression on CD44v6 level (Fig. 7h). These results were further supported by bioinformatics analysis showing that the levels of PRPF19 and other protein components in PRPF19/CDC5L complex are negatively correlated with the ratio of levels of CD44s/CD44v in LUADs, but not in LUSCs (Supplementary Fig. 7b–f). All together, our results suggested that the increase of USP15 protein nuclear localization and its interaction with PRPF19 plays a critical role in CD44v6 up-regulation mediated by ABHD11-AS1.

3.7. Up-regulation of CD44v6 by ABHD11-AS1 activates the Wnt/β-catenin pathway to promote tumorigenesis

We further investigated how ABHD11-AS1-up-regulated CD44v6 expression promotes lung carcinogenesis. Several studies showed that CD44v6 expression is associated with the activation of Wnt/β-catenin signaling pathway, one of key pathways involved in cancer stemness and tumorigenesis (Ghatak et al., 2022; Todaro et al., 2014). To further strengthen our ABHD11-AS1 findings, we next performed GSEA and found that gene sets involved in Wnt signaling pathway and pluripotency were significantly enriched in Cr(VI)-transformed cells (Supplementary Fig. 8a). On the other hand, knockdown of USP15 or PRPF19 in depleted these gene sets (Supplementary Fig. 8b and 8c). Our IF staining data also provided the evidence that ABHD11-AS1 over-expression in non-transformed human bronchial epithelial cells or HCC15 cells could promote β-catenin nuclear localization (Supplementary Fig. 9a), a hallmark of β-catenin activation. These results were further confirmed by Western blot analysis showing that stably overexpression of ABHD11-AS1 significantly increased active β-catenin levels whereas stably expressing ABHD11-AS1-as significantly reduced both total and active β-catenin level in lung cancer cells (Supplementary Fig. 9b to 9d).

Finally, we assessed the effect of manipulating CD44v6 on β-catenin subcellular localization, expression level and its functional outcomes. Our IF data showed that knockdown of CD44v6 in ABHD11-AS1-overexpressing non-transformed human bronchial epithelial cells or A549 cells drastically reduced β-catenin nuclear localization (Fig. 8a and 8b). Western blot analyses also showed that CD44v6 knockdown in these cells reduced active β-catenin levels (Fig. 8c). In addition, knockdown of USP15 or PRPF19 drastically decreased CD44, CD44v6, total and active β-catenin levels in A549 cells. However, stably overexpressing CD44 variants including CD44v6 was capable of rescuing the down-regulation of total and active β-catenin levels caused by USP15 or PRPF19 knockdown (Fig. 8d). Furthermore, silence of USP15 or PRPF19 in ABHD11-AS1-overexpressing HCC15 cells also reduced CD44, CD44v6, total and active β-catenin levels, and these effects were partially reversed by CD44v6 overexpression (Fig. 8d). Our data provided additional evidence for CD44v6 activating β-catenin pathway.

As shown in Supplementary Fig. 1, stably expressing ABHD11-AS1-as in H460 cells significantly reduced their tumorigenicity. Strikingly, stably overexpressing CD44 variants including CD44v6 in H460-ABHD11-AS1-as cells reversed the inhibitory effect of ABHD11-AS1-as overexpression on CSC-like property and tumorigenicity, as evidenced by forming significantly more suspension spheres, more and larger tumors in mice (Fig.

8e and 8f). Taken together, our findings suggested that CD44v6 plays an essential role in ABHD11-AS1-promoted CSC-like property and tumorigenesis.

4. Discussion

Recent studies reported that ABHD11-AS1 up-regulation has been found in several types of cancer and may function as an oncogenic lncRNA (Golla et al., 2022). However, the role of ABHD11-AS1 in environmental carcinogenesis has not been investigated. In addition, cancer subtype-specific expression pattern and the underlying mechanism of how ABHD11-AS1 may exhibit its oncogenic effect remain largely unexplored. In this study, we found that chronic Cr(VI) exposure up-regulated ABHD11-AS1 expression in cultured human bronchial epithelial cells and mouse lung tissues. Further functional and mechanistic studies revealed that up-regulation of ABHD11-AS1 contributes significantly to Cr(VI) exposure-induced cell malignant transformation, CSC-like property and tumorigenesis. These findings provided the first evidence showing that ABHD1-AS1 may play important roles in environmental carcinogenesis. Moreover, we also found that ABHD11-AS1 levels were up-regulated in lung adenocarcinomas (LUADs), but not in lung squamous cell carcinomas (LUSCs). By using Cr(VI)-transformed human bronchial epithelial cells, well-established human lung cancer cells, and bioinformatics analyses of lung cancer gene expression profiles, we demonstrated that up-regulation of ABHD11-AS1 plays crucial roles in both early and later stages of lung carcinogenesis. Our RNA pulldown assay coupled with mass spectrometric characterization unraveled that ABHD11-AS1 directly binds to SART3. Functional and mechanistic studies revealed that ABHD11-AS1-SART3 interaction enhanced USP15 nuclear localization, regulating CD44 RNA alternative splicing and promoting lung carcinogenesis.

Proper subcellular localization of proteins is important for maintaining normal functions whereas dysregulation of their localizations plays important roles in cancer. Among diverse mechanisms that regulate protein cellular localizations, the interactions between lncRNAs and proteins represent an important mechanism that relocates proteins from one subcellular compartment to another (Shaath et al., 2022; Schmitt and Chang, 2016; Wang et al., 2011). Thus, identifying novel protein-binding partners for lncRNAs is critical to further elucidate their biological functions and the underlying mechanisms. Xue et al. and Zeng et al. reported that EZH2 (Enhancer of Zeste Homolog 2) interacts with ABHD11-AS1 in human lung and ovarian cancer cells by using RNA immunoprecipitation (RIP) with an anti-EZH2 antibody followed by qPCR analysis (Xue et al., 2021; Zeng et al., 2019). Another study also showed that ABHD11-AS1 may interact with cyclin D1 in mouse xenograft tumors produced by injection of ABHD11-AS1-overexpressing human endometrial cancer cells (Liu et al., 2018). Our finding that the oncogenic lncRNA ABHD11-AS1 interacts with SART3 is significant at least in the following three aspects: (i) We performed RNA pulldown assays with both ABHD11-AS1 and its antisense RNA (as a negative control), and a specific interaction between ABHD11-AS1 and SART3 was identified by mass spectrometric analysis, and confirmed by Western blot analysis. Our finding demonstrated that ABHD11-AS1 directly and specifically binds to SART3; (ii) Previous studies reported that SART3 interacts with deubiquitinase USP15 and promotes USP15 nuclear localization to regulate RNA alternative splicing. Our findings indicated that the interaction between

ABHD11-AS1 and SART3 plays a pivotal role in promoting USP15 nuclear localization. (iii) This direct interaction between ABHD11-AS1 and SART3 which promotes USP15 nuclear localization to regulate RNA alternative splicing represents an important mechanism for the oncogenic effect of ABHD11-AS1.

Precise RNA alternative splicing is essential for gene regulations and biological functions whereas abnormal patterns of splicing events are highly involved in disease development and progression, especially in human cancers (Marasco & Kornblihtt, 2022; Ebrahimie et al., 2021; El Marabti & Younis, 2018). Our findings that increased nuclear deubiquitinase USP15 level and its interaction with and stabilizing splicing factor PRPF19 mediate the effect of ABHD11-AS1 on CD44 RNA splicing are significant at least in the following three aspects: (i) While aberrant RNA splicing is known to play some roles in carcinogenesis, the underlying mechanisms of how RNA splicing is deregulated in the carcinogenic process has not been well understood. This study provides new evidence supporting a crucial role of an oncogenic lncRNA in regulating RNA splicing to promote carcinogenesis; (ii) CD44 is a well-recognized CSC marker and up-regualtion of CD44 variants especially CD44v6 can promote cancer stemness. Notably, studies showed that expression of CD44 variants could be controlled by transcription factors, protein kinases and miRNAs (Hassn Mesrati et al., 2021). Here, we revealed a previously unknown mechanism for CD44v6 regulation by an oncogenic lncRNA ABHD11-AS1; (iii) Up-regulation of CD44 and CD44 variants is mainly found in cancer cells and tissues, supporting their roles in promoting cancer progression. Our study provided evidence showing that CD44v6 is significantly increased in a carcinogen-transformed human bronchial epithelial cells, implying that aberrant CD44 RNA splicing may happen in the early stage of carcinogenesis and play a key role in cell malignant transformation and CSC-like cell growth to promote cancer development.

Several oncogenic signaling pathways are activated down-stream of CD44v6 (Ma et al., 2019; Wang et al., 2018b). Our study provided additional data demonstrating that CD44v6 is capable of activating Wnt/β-catenin pathway, one of the major signaling pathways that promote cancer stemness and tumorigenesis. Our results indicated that ABHD11-AS1 activates Wnt/β-catenin pathway through regulating CD44 RNA alternative splicing to increase CD44v6 level, providing another mechanism for understanding how ABHD11-AS1 enhances cancer stemness to promote cancer development and progression.

Importantly, several studies reported that up-regulation of ABHD11-AS1 may serve as a potential biomarker for cancer diagnosis and prediction of cancer prognosis (Liu et al., 2019; Qiao et al., 2018; Yang et al., 2016; Lin et al., 2014]. However, no studies addressed any cancer subtype-specific expression of ABHD11-AS1. Our study clearly showed that ABHD11-AS1 is up-regulated in LUAD cells and tissues, but not in LUSC. As a result, high level of ABHD11-AS1 is correlated with a significantly worse overall survival in LUAD patients, but not in LUSC patients. Moreover, our ROC curve analysis suggests that high ABHD11-AS1 level may serve as a potential biomarker for diagnosis of LUADs, but not for LUSCs. These findings all indicated that ABHD11-AS1 may possess cancer subtype-specific oncogenic functions. Further mechanistic studies are needed to determine how ABHD11-AS1 level is specifically up-regulated in LUADs, which may establish ABHD11-AS1 as a new therapeutic target for patients with LUAD.

In summary, the findings from our study conclude that the oncogenic lncRNA ABHD11-AS1 is up-regulated at both early and later stages of lung carcinogenesis, interacting with SART3, and regulating CD44 RNA alternative splicing to promote lung cancer development and progression.

Supplementary Material

Refer to Web version on PubMed Central for supplementary material.

Funding

This work was supported by the National Institutes of Environmental Health Sciences (R01ES026151, R01ES029496, R01ES029942, and 1R01ES032787).

Data availability

Data will be made available on request.

References

Adnane S, Marino A, Leucci E, 2022. LncRNAs in human cancers: signal from noise. Trends Cell Biol. 32, 565–573. [PubMed: 35168846]

ATSDR (Agency for Toxic Substances and Disease Research), 2022. The ATSDR 2022 Substance Priority List. https://www.atsdr.cdc.gov/spl/#2022spl (accessed September 4, 2023).

Bell M, Schreiner S, Damianov A, Reddy R, Bindereif A, 2002. p110, a novel human U6 snRNP protein and U4/U6 snRNP recycling factor. EMBO J. 21, 2724–2735. [PubMed: 12032085]

Chen QY, Murphy A, Sun H, Costa M, 2019. Molecular and epigenetic mechanisms of Cr (VI)-induced carcinogenesis. Toxicol. Appl. Pharmacol. 377, 114636. [PubMed: 31228494]

Chen C, Zhao S, Karnad A, Freeman JW, 2018. The biology and role of CD44 in cancer progression: therapeutic implications. J. Hematol. Oncol. 11, 1–23. [PubMed: 29298689]

Clementino M, Xie J, Yang P, Li Y, Lin H-P, Fenske WK, Tao H, Kondo K, Yang C, Wang Z, 2020. A positive feedback loop between c-Myc upregulation, glycolytic shift, and histone acetylation enhances cancer stem cell-like property and tumorigenicity of Cr (VI)-transformed cells. Toxicol. Sci. 177, 71–83. [PubMed: 32525551]

Das T, Park JK, Park J, Kim E, Rape M, Kim EE, Song EJ, 2017. USP15 regulates dynamic protein–protein interactions of the spliceosome through deubiquitination of PRP31. Nucleic Acids Res. 45, 4866–4880. [PubMed: 28088760]

Das T, Kim EE, Song EJ, 2019. Phosphorylation of USP15 and USP4 regulates localization and spliceosomal deubiquitination. J. Mol. Biol. 431, 3900–3912. [PubMed: 31330151]

Delás MJ, Hannon GJ, 2017. lncRNAs in development and disease: from functions to mechanisms. Open Biol. 7, 170121. [PubMed: 28747406]

Dey BK, Mueller AC, Dutta A, 2014. Long non-coding RNAs as emerging regulators of differentiation, development, and disease. Transcription 5, e944014. [PubMed: 25483404]

Ebrahimie E, Rahimirad S, Tahsili M, Mohammadi-Dehcheshmeh M, 2021. Alternative RNA splicing in stem cells and cancer stem cells: importance of transcript-based expression analysis. World Journal of Stem Cells 13, 1394. [PubMed: 34786151]

El Marabti E, Younis I, 2018. The cancer spliceome: reprograming of alternative splicing in cancer. Front. Mol. Biosci. 5, 80. [PubMed: 30246013]

Frankish A, Diekhans M, Jungreis I, Lagarde J, Loveland JE, Mudge JM, Sisu C, Wright JC, Armstrong J, Barnes I, 2021. GENCODE 2021. Nucleic Acids Res. 49, D916–D923. [PubMed: 33270111]

Ghatak S, Hascall VC, Karamanos N, Markwald RR, Misra S, 2022. Chemotherapy induces feedback up-regulation of CD44v6 in colorectal cancer initiating cells through β-catenin/MDR1 signaling to sustain chemoresistance. Front. Oncol. 12, 906260. [PubMed: 36330477]

Golla U, Sesham K, Dallavalasa S, Manda NK, Unnam S, Sanapala AK, Nalla S, Kondam S, Kumar R, 2022. ABHD11-AS1: an emerging long non-coding RNA (lncRNA) with clinical significance in human malignancies. Non-Coding RNA 8, 21. [PubMed: 35314614]

Grote M, Wolf E, Will CL, Lemm I, Agafonov DE, Schomburg A, Fischle W, Urlaub H, Lührmann R, 2010. Molecular architecture of the human Prp19/CDC5L complex. Mol. Cell. Biol. 30, 2105–2119. [PubMed: 20176811]

Hassn Mesrati M, Syafruddin SE, Mohtar MA, Syahir A, 2021. CD44: A multifunctional mediator of cancer progression. Biomolecules 11, 1850. [PubMed: 34944493]

Herman AB, Tsitsipatis D, Gorospe M, 2022. Integrated lncRNA function upon genomic and epigenomic regulation. Mol. Cell 82, 2252–2266. [PubMed: 35714586]

IARC (International Agency for Research on Cancer). Chromium, nickel and welding. IARC Monograph on the Evaluation of Carcinogenic Risks to Humans. World Health Organization, Lyon, France 1990.

Kamelgarn M, Chen J, Kuang L, Jin H, Kasarskis EJ, Zhu H, 2018. ALS mutations of FUS suppress protein translation and disrupt the regulation of nonsense-mediated decay. Proc. Nat. Acad. Sci. 115, E11904–E11913. [PubMed: 30455313]

Khawar MB, Hamid SE, Jan T, Abbasi MH, Idnan M, Sheikh N, 2022. Diagnostic, prognostic and therapeutic potential of long noncoding RNAs in cancer. Mol. Biol. Rep. 49, 2311–2319. [PubMed: 35072835]

Kouokam JC, Meaza I, Wise JP Sr, 2022. Inflammatory effects of hexavalent chromium in the lung: A comprehensive review. Toxicol. Appl. Pharmacol. 455, 116265. [PubMed: 36208701]

Li C, Tang Z, Zhang W, Ye Z, Liu F, 2021. GEPIA2021: integrating multiple deconvolution-based analysis into GEPIA. Nucleic Acids Res. 49, W242–W246. [PubMed: 34050758]

Lin X, Yang M, Xia T, Guo J, 2014. Increased expression of long noncoding RNA ABHD11-AS1 in gastric cancer and its clinical significance. Med. Oncol. 31, 1–5.

Liu SJ, Dang HX, Lim DA, Feng FY, Maher CA, 2021. Long noncoding RNAs in cancer metastasis. Nat. Rev. Cancer 21, 446–460. [PubMed: 33953369]

Liu Y, Wang LL, Chen S, Zong ZH, Guan X, Zhao Y, 2018. LncRNA ABHD11-AS1 promotes the development of endometrial carcinoma by targeting cyclin D1. J. Cell Mol. Med. 22, 3955–3964. [PubMed: 29799152]

Liu Y, Feng W, Liu W, Kong X, Li L, He J, Wang D, Zhang M, Zhou G, Xu W, 2019. Circulating lncRNA ABHD11-AS1 serves as a biomarker for early pancreatic cancer diagnosis. J. Cancer 10, 3746. [PubMed: 31333792]

Ma L, Dong L, Chang P, 2019. CD44v6 engages in colorectal cancer progression. Cell Death Dis. 10, 30. [PubMed: 30631039]

Marasco LE, Kornblihtt AR, 2023. The physiology of alternative splicing. Nat. Rev. Mol. Cell Biol. 24, 242–254. [PubMed: 36229538]

Mattick JS, Amaral PP, Carninci P, Carpenter S, Chang HY, Chen L-L, Chen R, Dean C, Dinger ME, Fitzgerald KA, 2023. Long non-coding RNAs: definitions, functions, challenges and recommendations. Nat. Rev. Mol. Cell Biol. 24, 430–447. [PubMed: 36596869]

Nojima T, Proudfoot NJ, 2022. Mechanisms of lncRNA biogenesis as revealed by nascent transcriptomics. Nat. Rev. Mol. Cell Biol. 23, 389–406. [PubMed: 35079163]

Qiao X, Lv S-X, Qiao Y, Li Q-P, Ye B, Wang C-C, Miao L, 2018. Long noncoding RNA ABHD11-AS1 predicts the prognosis of pancreatic cancer patients and serves as a promoter by activating the PI3K-AKT pathway Eur. Rev. Med. Pharmacol. Sci. 22.

Schmitt AM, Chang HY, 2016. Long noncoding RNAs in cancer pathways. Cancer Cell 29, 452–463. [PubMed: 27070700]

Shaath H, Vishnubalaji R, Elango R, Kardousha A, Islam Z, Qureshi R, Alam T, Kolatkar PR, Alajez NM, 2022. Long non-coding RNA and RNA-binding protein interactions in cancer: Experimental and machine learning approaches. Seminars in Cancer Biology: Elsevier.

Tang Z, Li C, Kang B, Gao G, Li C, Zhang Z, 2017. GEPIA: a web server for cancer and normal gene expression profiling and interactive analyses. Nucleic Acids Res. 45, W98–W102. [PubMed: 28407145]

Todaro M, Gaggianesi M, Catalano V, Benfante A, Iovino F, Biffoni M, Apuzzo T, Sperduti I, Volpe S, Cocorullo G, 2014. CD44v6 is a marker of constitutive and reprogrammed cancer stem cells driving colon cancer metastasis. Cell Stem Cell 14, 342–356. [PubMed: 24607406]

Wang KC, Chang HY, 2011. Molecular mechanisms of long noncoding RNAs. Mol. Cell 43, 904–914. [PubMed: 21925379]

Wang Z, Yang J, Fisher T, Xiao H, Jiang Y, Yang C, 2012. Akt activation is responsible for enhanced migratory and invasive behavior of arsenic-transformed human bronchial epithelial cells. Environ. Health Perspect. 120, 92–97. [PubMed: 21954225]

Wang Z, Humphries B, Xiao H, Jiang Y, Yang C, 2013. Epithelial to mesenchymal transition in arsenic-transformed cells promotes angiogenesis through activating β-catenin–vascular endothelial growth factor pathway. Toxicol. Appl. Pharmacol. 271, 20–29. [PubMed: 23643801]

Wang Z, Humphries B, Xiao H, Jiang Y, Yang C, 2014. MicroRNA-200b suppresses arsenic-transformed cell migration by targeting protein kinase Cα and Wnt5b-protein kinase Cα positive feedback loop and inhibiting Rac1 activation. J. Biol. Chem. 289, 18373–18386. [PubMed: 24841200]

Wang Z, Wu J, Humphries B, Kondo K, Jiang Y, Shi X, Yang C, 2018a. Upregulation of histone-lysine methyltransferases plays a causal role in hexavalent chromium-induced cancer stem cell-like property and cell transformation. Toxicol. Appl. Pharmacol. 342, 22–30. [PubMed: 29391238]

Wang Z, Zhao K, Hackert T, Zöller M, 2018b. CD44/CD44v6 a reliable companion in cancer-initiating cell maintenance and tumor progression. Front. Cell Dev. Biol. 6, 97. [PubMed: 30211160]

Wang Z, Li Y, Xiao Y, Lin HP, Yang P, Humphries B, Gao T, Yang C, 2019a. Integrin α9 depletion promotes β-catenin degradation to suppress triple-negative breast cancer tumor growth and metastasis. Int. J. Cancer 145, 2767–2780. [PubMed: 31008533]

Wang P-S, Wang Z, Yang C, 2021. Dysregulations of long non-coding RNAs–the emerging “lnc” in environmental carcinogenesis. Seminars in Cancer Biology: Elsevier.

Wang Z, Yang C, 2019. Metal carcinogen exposure induces cancer stem cell-like property through epigenetic reprograming: A novel mechanism of metal carcinogenesis. Seminars in Cancer Biology: Elsevier.

Wang Z, Yang C, 2023. Epigenetic and epitranscriptomic mechanisms of chromium carcinogenesis. Advances in Pharmacology: Elsevier.

Wang Z, Lin H-P, Li Y, Tao H, Yang P, Xie J, Maddy D, Kondo K, Yang C, 2019b. Chronic hexavalent chromium exposure induces cancer stem cell-like property and tumorigenesis by increasing c-Myc expression. Toxicol. Sci. 172, 252–264. [PubMed: 31504995]

Wang Z, Yang P, Xie J, Lin H-P, Kumagai K, Harkema J, Yang C, 2020. Arsenic and benzo [a] pyrene co-exposure acts synergistically in inducing cancer stem cell-like property and tumorigenesis by epigenetically down-regulating SOCS3 expression. Environ. Int. 137, 105560. [PubMed: 32062438]

Wang Z, Uddin MB, Xie J, Tao H, Zeidler-Erdely PC, Kondo K, Yang C, 2022. Chronic hexavalent chromium exposure upregulates the RNA methyltransferase METTL3 expression to promote cell transformation, cancer stem cell-like property, and tumorigenesis. Toxicol. Sci. 187, 51–61. [PubMed: 35201342]

Wen J, Wang H, Dong T, Gan P, Fang H, Wu S, Li J, Zhang Y, Du R, Zhu Q, 2019. STAT3-induced upregulation of lncRNA ABHD11-AS1 promotes tumour progression in papillary thyroid carcinoma by regulating miR-1301–3p/STAT3 axis and PI3K/AKT signalling pathway. Cell Prolif. 52, e12569. [PubMed: 30657221]

Xiao Y, Li Y, Tao H, Humphries B, Li A, Jiang Y, Yang C, Luo R, Wang Z, 2018. Integrin α5 down-regulation by miR-205 suppresses triple negative breast cancer stemness and metastasis by inhibiting the Src/Vav2/Rac1 pathway. Cancer Lett. 433, 199–209. [PubMed: 29964204]

Xue L, Li J, Lin Y, Liu D, Yang Q, Jian J, Peng J, 2021. m6A transferase METTL3-induced lncRNA ABHD11-AS1 promotes the Warburg effect of non-small-cell lung cancer. J. Cell. Physiol. 236, 2649–2658. [PubMed: 32892348]

Yan Y, Zuo X, Wei D, 2015. Concise review: emerging role of CD44 in cancer stem cells: a promising biomarker and therapeutic target. Stem Cells Transl. Med. 4, 1033–1043. [PubMed: 26136504]

Yang Y, Shao Y, Zhu M, Li Q, Yang F, Lu X, Xu C, Xiao B, Sun Y, Guo J, 2016. Using gastric juice lncRNA-ABHD11-AS1 as a novel type of biomarker in the screening of gastric cancer. Tumor Biol. 37, 1183–1188.

Yang C, Wang Z, 2022. The epitranscriptomic mechanism of metal toxicity and carcinogenesis. Int. J. Mol. Sci. 23, 11830. [PubMed: 36233132]

Yang C, Wu J, Zhang R, Zhang P, Eckard J, Yusuf R, Huang X, Rossman TG, Frenkel K, 2005. Caffeic acid phenethyl ester (CAPE) prevents transformation of human cells by arsenite (As) and suppresses growth of As-transformed cells. Toxicology 213, 81–96. [PubMed: 16085347]

Yatera K, Morimoto Y, Ueno S, Noguchi S, Kawaguchi T, Tanaka F, Suzuki H, Higashi T, 2018. Cancer risks of hexavalent chromium in the respiratory tract. J. UOEH 40, 157–172. [PubMed: 29925735]

Zeidler-Erdely PC, Falcone LM, Antonini JM, Fraser K, Kashon ML, Battelli LA, Salmen R, Trainor T, Grose L, Friend S, 2020. Tumorigenic response in lung tumor susceptible A/J mice after sub-chronic exposure to calcium chromate or iron (III) oxide. Toxicol. Lett. 334, 60–65. [PubMed: 32961271]

Zeng XY, Jiang XY, Yong JH, Xie H, Yuan J, Zeng D, Dou YY, Xiao SS, 2019. lncRNA ABHD11-AS1, regulated by the EGFR pathway, contributes to the ovarian cancer tumorigenesis by epigenetically suppressing TIMP2. Cancer Med. 8, 7074–7085. [PubMed: 31568657]

Zhang Q, Harding R, Hou F, Dong A, Walker JR, Bteich J, Tong Y, 2016. Structural basis of the recruitment of ubiquitin-specific protease USP15 by spliceosome recycling factor SART3. J. Biol. Chem. 291, 17283–17292. [PubMed: 27255711]

Zhu Y, Costa M, 2020. Metals and molecular carcinogenesis. Carcinogenesis 41, 1161–1172. [PubMed: 32674145]

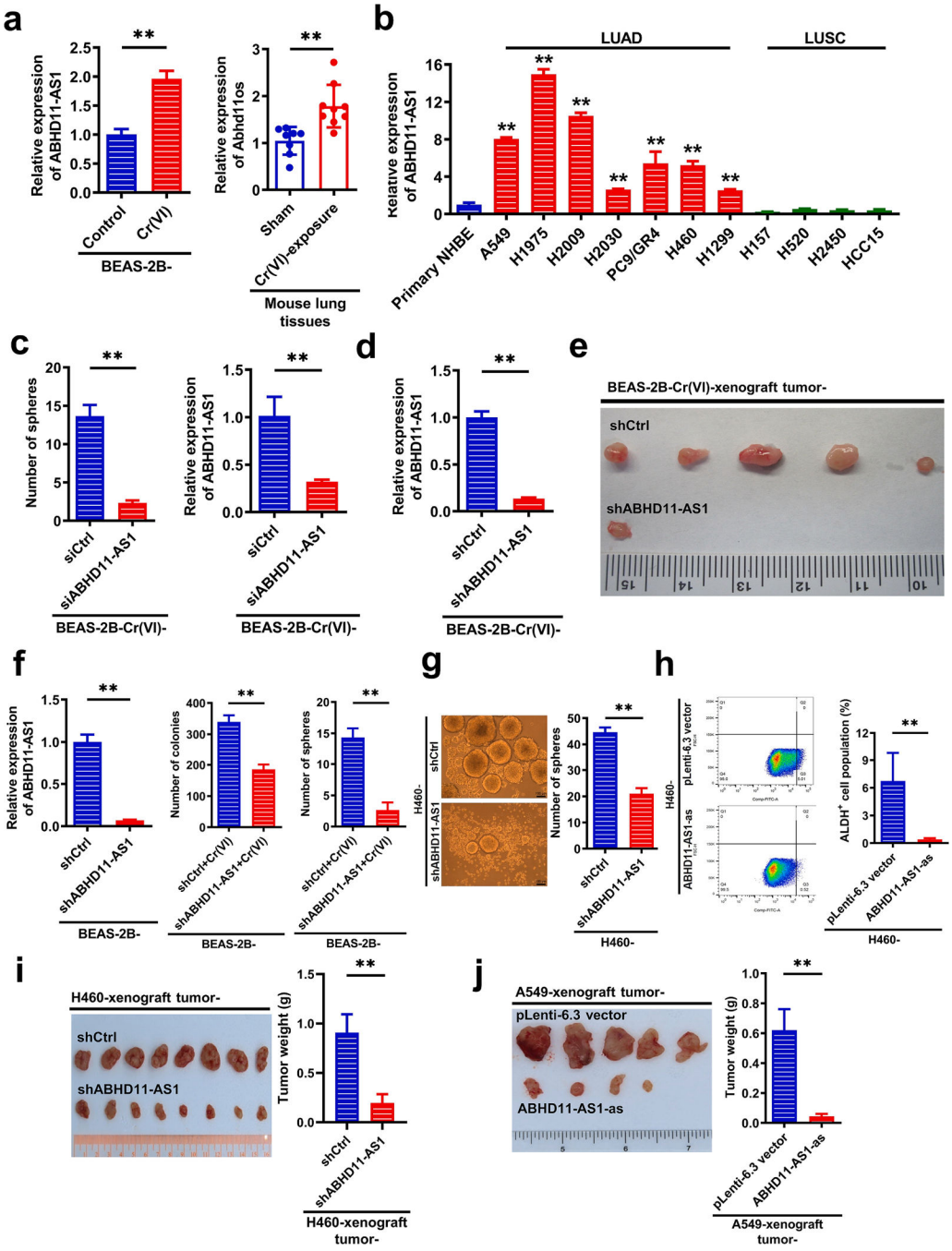

Fig. 1.

ABHD11-AS1 levels are up-regulated in different stages of lung carcinogenesis playing an important role in tumorigenesis. **a** AHBD11-AS1 expression level in Cr(VI)-transformed cells (n = 3) and chronic Cr(VI)-exposed mouse lung tissues (n = 9). **b** AHBD11-AS1 expression level in LUAD and LUSC cells (n = 3). **c** Effect of siRNA knockdown of ABHD11-AS1 in Cr(VI)-transformed cells on their capability of forming suspension spheres (n = 3). **d-e** Effect of stably knocking down of ABHD11-AS1 in Cr(VI)-transformed cells on their capability of growing xenograft tumors in nude mice (n = 5). **f** Effect of stably

knocking down of ABHD11-AS1 in parental non-transformed human bronchial epithelial cells on chronic Cr(VI) exposure-induced soft agar colony and suspension culture sphere formation (n = 3). **g** Effect of stably knocking down ABHD1-AS1 in lung cancer H460 cells on their capability of growing suspension spheres (n = 3). **h** Effect of stably expressing antisense RNA of ABHD11-AS1 (ABHD11-AS1-as) in H460 cells on their ALDH activity (n = 5). **i** Effect of stably knocking down ABHD11-AS1 in H460 cells on xenograft tumor growth in nude mice (n = 8). **j** Effect of stably expressing ABHD11-AS1-as in A549 cells on xenograft tumor growth in nude mice (n = 5). ** $p < 0.01$.

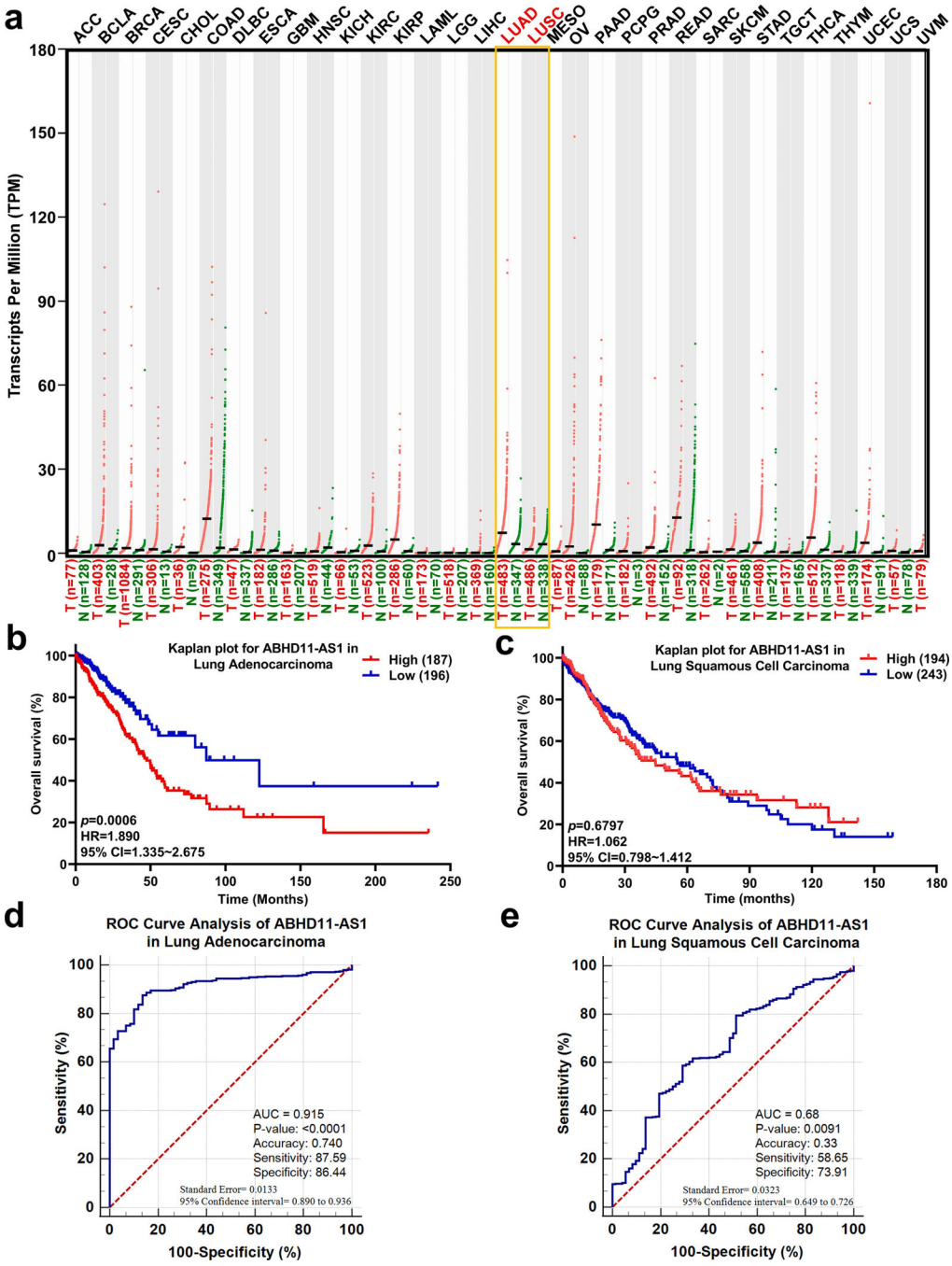

Fig. 2.

ABHD11-AS1 levels are up-regulated and associated with worse prognosis in lung adenocarcinomas but not in lung squamous cell carcinomas. **a** Online Gene Expression Profiling Interactive Analysis (http://gepia.cancer-pku.cn/) of ABHD11-AS1 levels in various normal and cancer tissues. **b-c** Bioinformatics analyses of the relationship between ABHD11-AS1 level and overall survival of LUAD (**b**) and LUSC (**c**) patients. **d-e** ROC curve analysis of diagnostic value of ABHD11-AS1 in LUADs (**d**) and LUSCs (**e**). The profile of ABHD11-AS1 in LUADs and LUSCs were obtained from

TCGA_LUAD (https://portal.gdc.cancer.gov/projects/TCGA-LUAD) and TCGA_LUSC (https://portal.gdc.cancer.gov/projects/TCGA-LUSC) project datasets and used for overall survival (**b-c**) and diagnostic analyses (**d-e**).

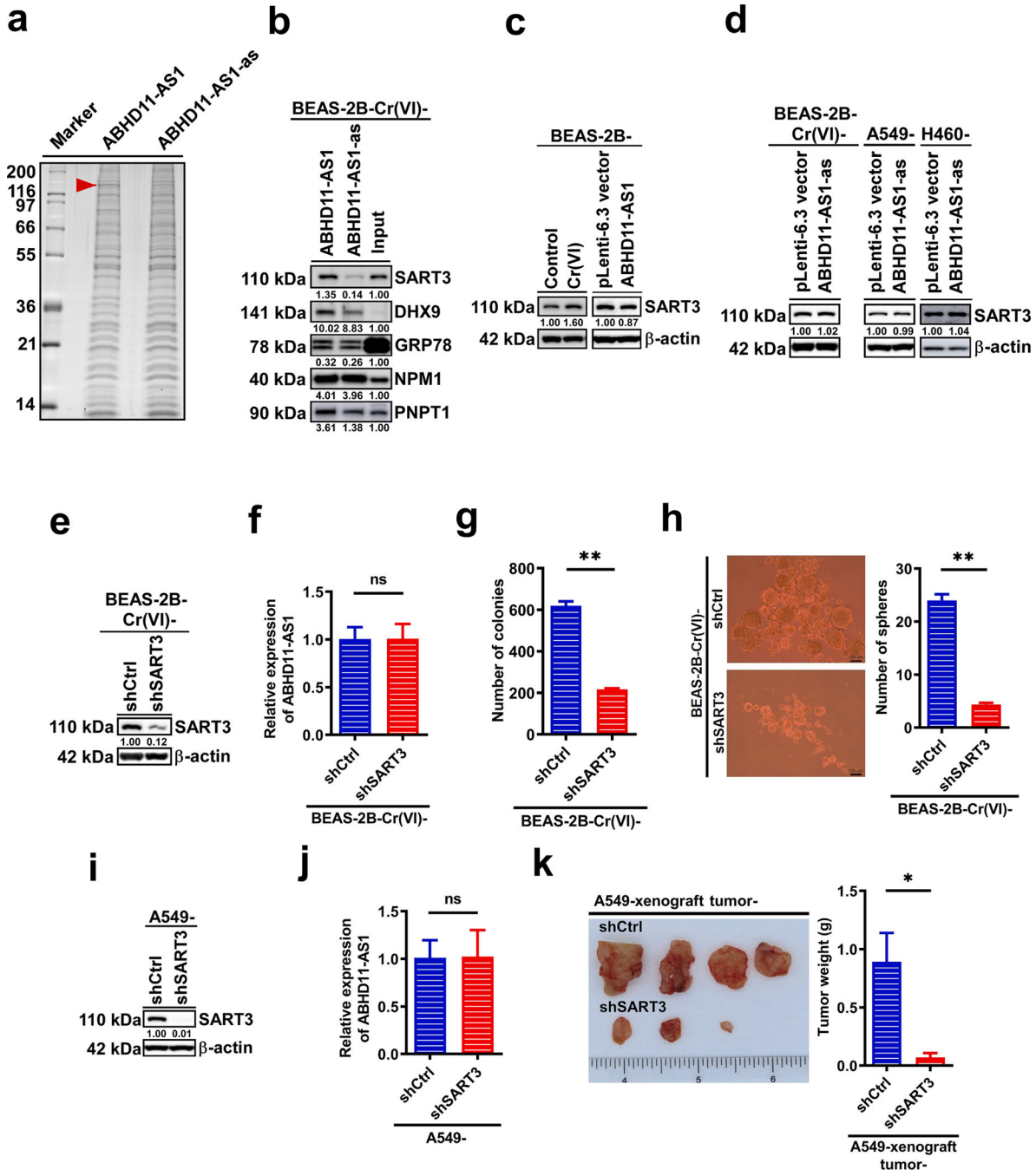

Fig. 3.

ABHD11-AS1 directly interacts with SART3 and knockdown of SART3 reduces malignant phenotypes of Cr(VI)-transformed cells and human lung cancer cells. **a** A representative protein gel from ABHD11-AS1 and its antisense RNA (ABHD11-AS1-as) pulldown assay. The red arrowhead points to a unique band from ABHD11-AS1 pulldown assay. **b** A representative Western blot confirmation of candidate proteins that interact with ABHD11-AS1 or ABHD11-AS1-as. Biotinylated ABHD11-AS1 or ABHD11-AS1-as were incubated with cell lysate of Cr(VI)-transformed cells and proceeded for RNA pulldown assays and

subsequent Western blot analysis to confirm the interaction partners of ABHD11-AS1. **c-e** Western blot analysis of SART3 in various cells. The numbers underneath each protein band are the ratios of the intensities of the protein band divided by the corresponding input protein band intensities or β-actin band intensities (as loading controls). **f** Effect of SART3 knockdown on ABHD11-AS1 level in Cr(VI)-transformed cells (n = 3). **g-h** Effect of SART3 knockdown on the numbers of soft agar colonies and suspension spheres formed by Cr(VI)-transformed cells (n = 3). **i-k** Effect of SART3 knockdown in A549 cells (**i**) on ABHD11-AS1 level (n = 3) (**j**) and xenograft tumor growth in nude mice (n = 4) (**k**). * $p < 0.05$; ** $p < 0.01$; ns: no significance.

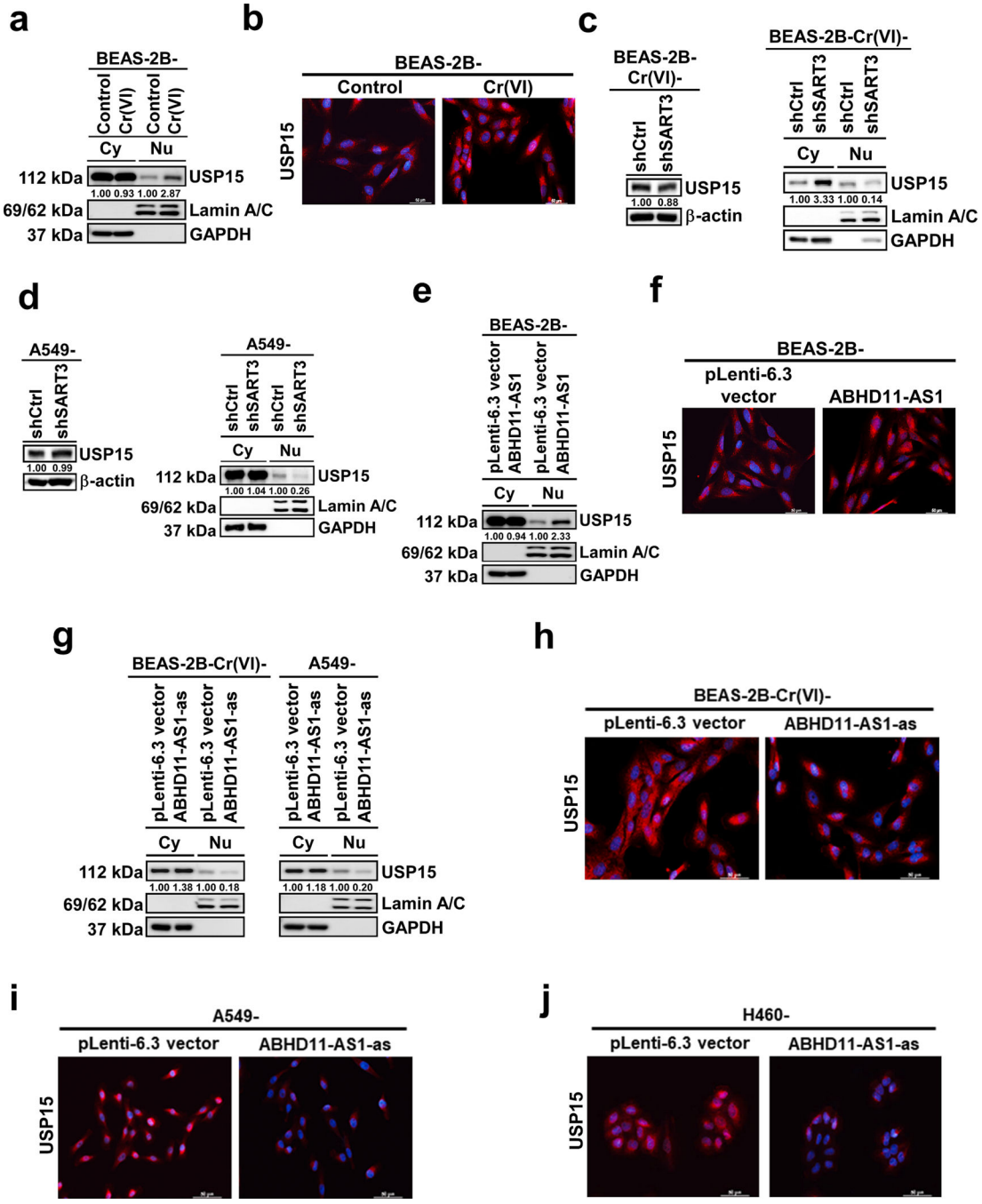

Fig. 4.

ABHD11-AS1 and SART3 interaction promotes USP15 nuclear localization. **a,c,d,e,g** Cell fractionation analysis of USP15 cytosol and nuclear distribution in various cells. The numbers underneath USP15 protein bands are ratios of each USP15 band intensity divided by the corresponding control protein band intensity. **b,f, h,i,j** The representative overlaid images of immunofluorescence (IF) staining of USP15 (red) and DNA DAPI (blue) staining in various cells. Scale bar: 50 μm.

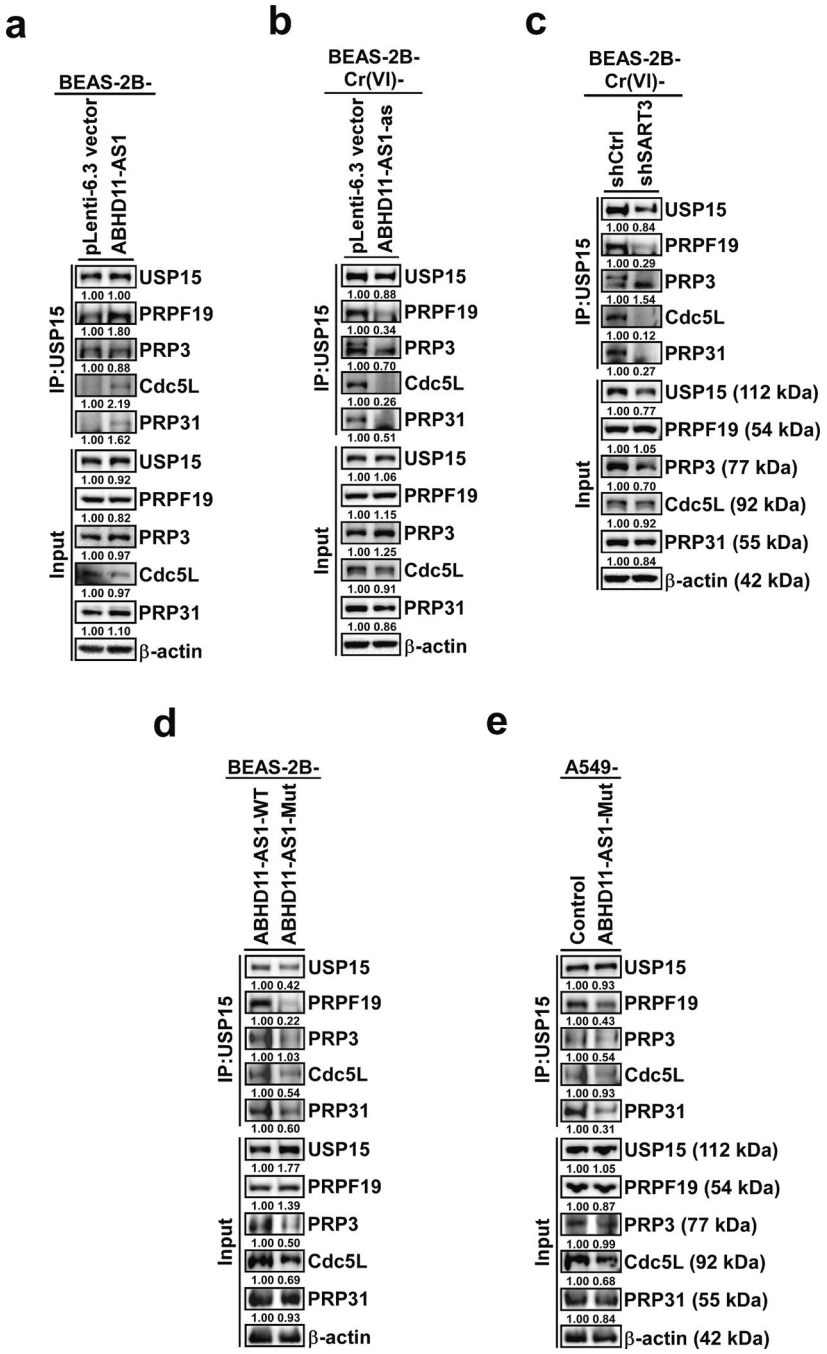

Fig. 5.

ABHD11-AS1 and SART3 increase the interaction of USP15 with RNA splicing factor PRPF19. **a,b,c,d,e** Co-immunoprecipitation (Co-IP) analysis of the interaction between USP15 and several splicing factors in whole cell lysates of BEAS-2B cells overexpressing ABHD11-AS1 (a), Cr(VI)-transformed cells overexpressing the antisense RNA of ABHD11-AS1 (b), Cr(VI)-transformed cells with SART3 stable knockdown (c), BEAS-2B cells overexpressing an ABHD11-AS1 wildtype and an mutant with SART3 binding site mutated (d), and A549 cells overexpressing an ABHD11-AS1 mutant with

SART3 binding site mutated (e). The numbers underneath each precipitated protein band are ratios of each precipitated protein band intensity divided by the corresponding input protein band intensity. The numbers underneath each input protein band are ratios of each input protein band intensity divided by the corresponding input β-actin protein band intensity.

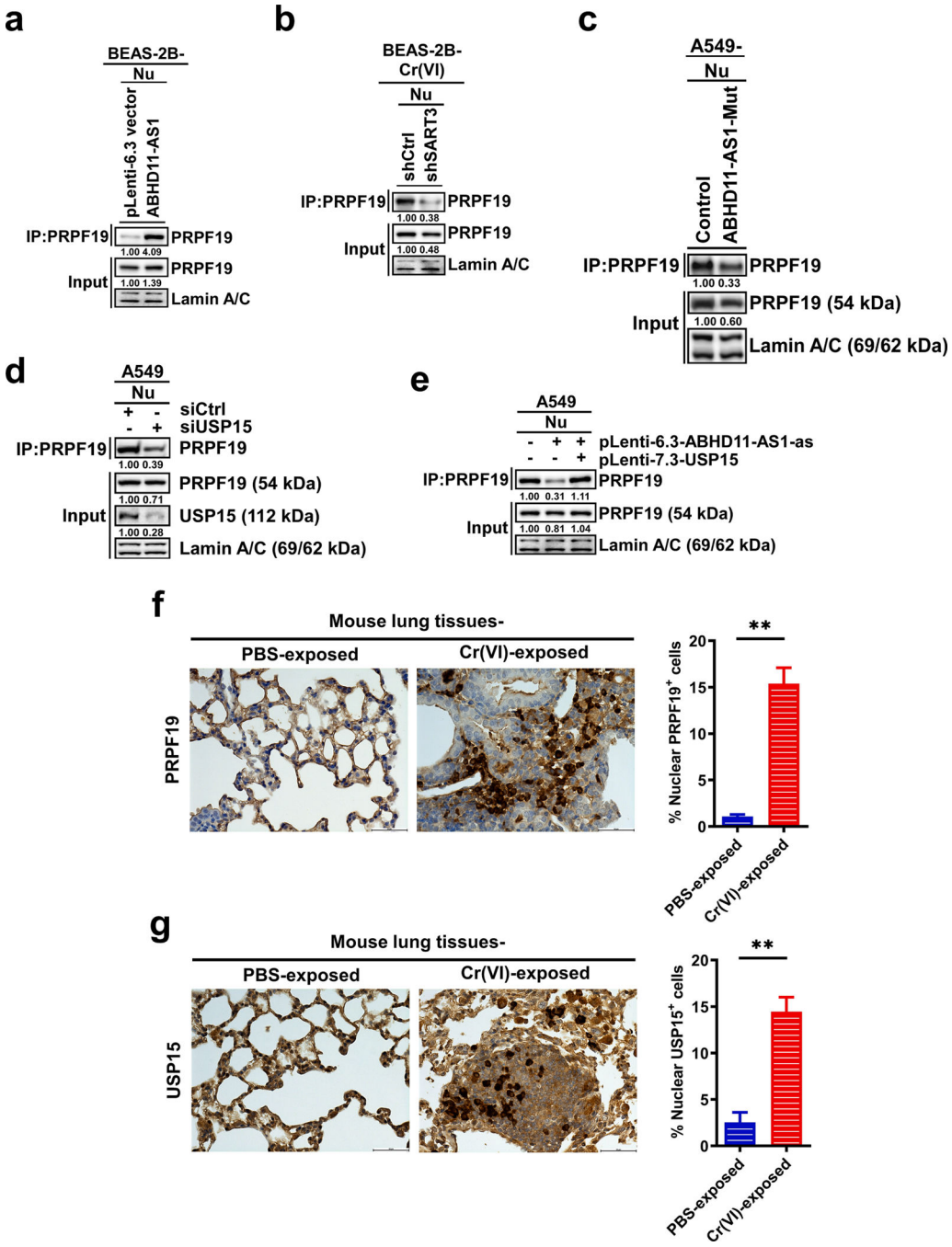

Fig. 6.

Stably expressing ABHD11-AS1 increases but knocking down SART3 or USP15 or stably expressing an ABHD11-AS1 mutant reduce RNA splicing factor PRPF19 protein level. **a,b,c,d,e** IP analysis of nuclear PRPF19 protein level in various cells. The numbers underneath the precipitated PRPF19 protein bands are ratios of immunoprecipitated PRPF19 band intensity divided by the input PRPF19 band intensity. The numbers underneath each input protein band are ratios of each input protein band intensity divided by the corresponding input β-actin protein band intensity. **f, g** Representative images of PRPF19 (f)

and USP15 (g) immunohistochemistry (IHC) staining in PBS-exposed normal mouse lung tissues and chronic Cr(VI) exposure-induced mouse lung tumor tissues, respectively. Scale bar: 50 μm.

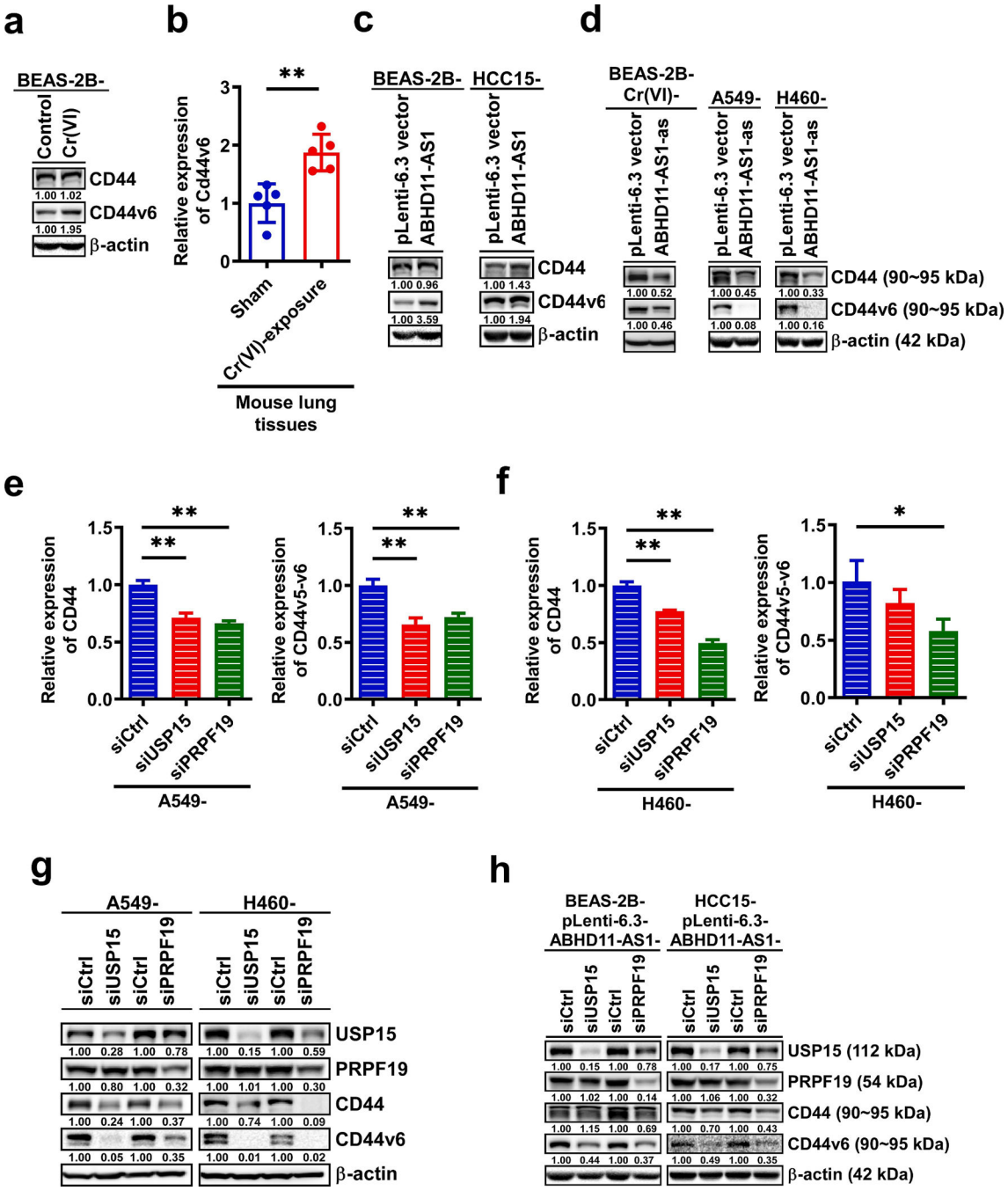

Fig. 7.

USP15 and PRPF19 mediate CD44v6 up-regulation by ABHD11-AS1. **a,c,d** Western blot analyses of CD44 and CD44v6 protein levels in various cells. **b** qPCR analysis of CD44v6 mRNA levels in PBS-exposed control mouse lungs and chronic Cr(VI)-exposed mouse lungs (n = 5). **e,f** qPCR analysis of CD44 and CD44v6 mRNA levels in A549 and H460 cells transfected with control siRNA, USP15 siRNA or PRPF19 siRNA (n = 3). **g** Western blot analysis of USP15, PRPF19, CD44 and CD44v6 protein levels in A549 and H460 cells transfected with control siRNA, USP15 siRNA or PRPF19 siRNA. **h** Western blot analysis

of USP15, PRPF19, CD44 and CD44v6 protein levels in ABHD11-AS1-overexpressing BEAS-2B and HCC15 cells transfected with control siRNA, USP15 siRNA or PRPF19 siRNA. * $p < 0.05$; ** $p < 0.01$.

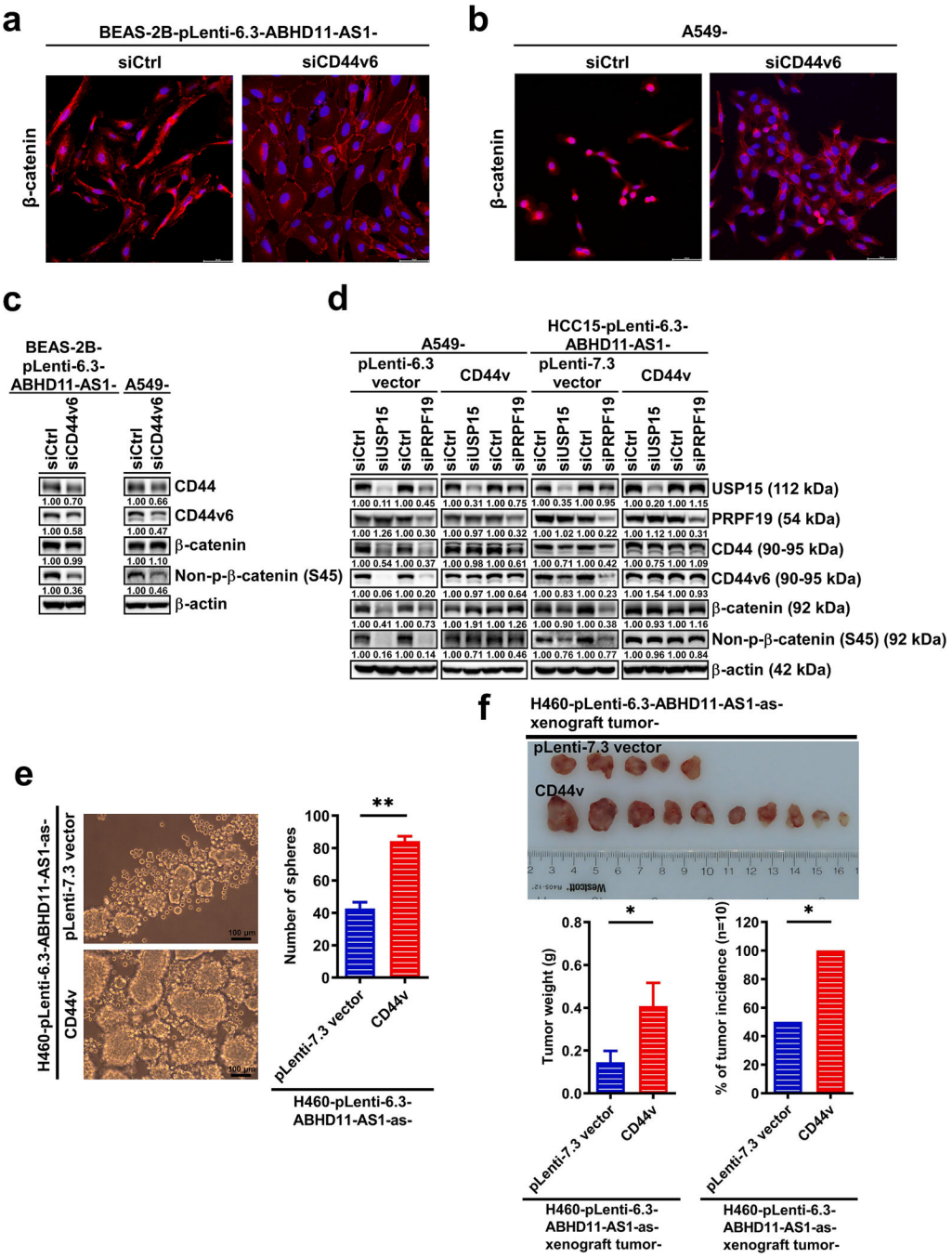

Fig. 8.

Up-regulation of CD44v6 by ABHD11-AS1 activates Wnt/β-catenin pathway to promote tumorigenesis. **a,b** Representative overlaid images of IF staining of β-catenin (red) and nuclear DAPI staining (blue) in BEAS-2B-ABHD11-AS1 and A549 cells transfected with control or CD44v6 targeting siRNAs. Scale bar: 50 μm. **c** Western blot analysis of the effect of siRNA targeting CD44v6 on total and active-β-catenin protein levels in BEAS-2B-ABHD11-AS1 and A549 cells. **d** Western blot analysis of the effect of siRNA targeting USP15 or PRP19 on total and active-β-catenin protein levels in vector control

and CD44 variants stably expressing A549 cells and HCC15-ABHD11-AS1 cells. **e** Effect of overexpressing CD44 variants on suspension sphere forming ability of ABHD11-AS1-as-overexpressing H460 cells. **f** Effect of overexpressing CD44 variants on the growth and incidence of nude mouse xenograft tumors produced by injection of ABHD11-AS1-as-overexpressing H460 cells (n = 10). * $p < 0.05$.